*J. Fluid Mech.* (1999), *vol.* 385, *pp.* 157–197. Printed in the United Kingdom



# Primary acoustic instability of flames propagating in tubes: cases of spray and premixed gas combustion

By CHRISTOPHE CLANET, GEOFFREY SEARBY AND PAUL CLAVIN

Institut de Recherche sur les Phénomènes Hors Équilibre, UMR 6594,
CNRS and Universities of Marseille I & II, Service 252, Campus de St. Jérôme,
13397 Marseille Cedex 20, France

(Received 17 December 1997 and in revised form 2 November 1998)

This paper is concerned with the coupling mechanisms leading to the spontaneous generation of sound during flame propagation in a tube open at one end. We consider the cases of premixed gaseous combustion and of premixed spray combustion of decane droplets in air. The flame front propagates from the open to the closed end of a tube and, for a particular position, starts to amplify a longitudinal acoustic mode of the tube. We call this mode the primary acoustic instability and focus our study on the physical mechanisms responsible for sound amplification. Measured amplification rates are compared to calculated values. In the gaseous case, it is shown that the instability results from a coupling between the acoustic acceleration field and the geometry of the flame front separating the burnt gases from the denser unburnt mixture. The situation is quite different in the spray case. The primary acoustic instability is much stronger and results from a modification of the inner structure of the flame. This modification arises from the velocity lag of the droplets in the acoustic velocity field, leading to a modulation of the fuel flux at the flame.

## 1. Introduction

The first experimental evidence of the thermo-acoustic instability of a flame propagating in a tube is found in the work of Mallard & Le Chatelier (1883). A recent experimental study of Searby (1992), which follows the previous work of Kaskan (1953), Markstein (1953) and Leyer & Manson (1971), describes the different phases of the development of the instability when a premixed flame propagates from the open to the closed end of a tube. It is now clear that the final phase is a violent parametric instability, first identified by Markstein (1964). This secondary parametric instability can be triggered only by pre-existing finite-amplitude acoustic oscillations (Searby & Rochwerger 1991). The primary acoustic instability is thus seen to be the key feature of the whole process.

Different mechanisms have been proposed by Dunlap (1950), Kaskan (1953), Rauschenbakh (1961) and Markstein (1970) to explain the primary acoustic instability. The theoretical work of Clavin, Pelcé & He (1990), considering Dunlap's mechanism, and Pelcé & Rochwerger (1992), considering Rauschenbakh's mechanism, give analytical expressions for the linear growth rate associated with these two mechanisms. More recently Clavin & Sun (1991) have proposed a new mechanism specific to premixed spray flames. However, up to now, the lack of precise experimental data has made it

impossible to identify the primary instability mechanism unambiguously. The main purpose of this paper is to provide such experimental data. We will use the comparison between the premixed gaseous case (propane–air mixture) and the premixed spray case (decane droplets in air) to help identify the physical mechanisms responsible for the primary sound emission in each case.

Acoustic instabilities in combustion result from a constructive coupling between local heat release fluctuations and pressure oscillations associated with the acoustic modes of the combustion chamber. A fluctuation of the reaction rate of quasi-isobaric combustion acts as an unsteady local source of volume which generates sound (Strahle 1985; Clavin & Siggia 1991). The loop is closed by a feedback mechanism in which the heat release rate is modulated by the action of the acoustic wave. According to Rayleigh's criterion (Rayleigh 1878), the instability develops if the local heat release rate fluctuation is in phase with the pressure oscillation of the acoustic wave. Several feedback mechanisms have been proposed. They can be classed into different categories according to whether they modify the local internal structure or the global geometry of the flame front and to whether they are related to the action of the acoustic pressure and temperature oscillations (*pressure coupling*), or to the action of the acoustic velocity (*velocity coupling*).

Dunlap (1950) first proposed a mechanism for flames in premixed gases. It involves the modulation of the reaction rate of the flame produced by the temperature fluctuations associated with an adiabatic acoustic wave. According to the terminology defined above, it is a pressure coupling mechanism involving the internal structure of the front. The theoretical analysis of Clavin *et al.* (1990) shows that the corresponding amplification can be just sufficient to overcome viscous and radiative damping and could lead to an instability, but only in some marginal cases.

Rauschenbakh (1961) and Markstein (1970) have proposed a different type of feed-back mechanism which can potentially lead to a much stronger instability: the difference of density between the hot burnt gases and the cold unburnt gases makes the shape of a curved flame front sensitive to the presence of an acceleration such as that associated with an acoustic velocity field. This mechanism is thus a velocity coupling involving the geometry of the front. The modulation of total energy release rate arises from the modulation of the total flame surface area produced by the action of the acoustic acceleration on the amplitude of cellular structures. The theoretical analysis of this mechanism is less advanced than the preceding one; however the analytical results of Pelcé & Rochwerger (1992), obtained in the limit of a weakly curved interface, give a correct estimation of the growth rate of this instability.

The experimental results presented in this paper for premixed gaseous flames show that the measured growth rate of the primary instability is between one and two orders of magnitude higher than that predicted for the pressure coupling mechanism described by Clavin *et al.* (1990), but is compatible with the growth rate calculated for the velocity coupling mechanism treated by Pelcé & Rochwerger (1992).

Additional results of this paper concern the primary acoustic instability of a flame propagating in a spray of decane droplets in air. The regime that is studied here will be called premixed spray combustion. In this regime the spray droplets are small, numerous and uniformly distributed in the unburnt gas, so that fuel mass fraction is constant when averaged over a fluid element whose size is of the same order as the flame thickness. Moreover in this regime the droplets vaporize on a time scale short compared to the transit time through the flame and the structure of the chemical reaction zone is similar to that of a premixed gaseous flame, see § 5. Our experimental measurements show that the linear growth rate

in the spray case is an order of magnitude higher than for the corresponding gaseous case. This result can be explained by the coupling mechanism proposed by Clavin & Sun (1991) for spray flames. This mechanism involves a modification of the internal structure of the flame in the presence of an acoustic wave. However, in the spray case, the change in internal structure is produced by the velocity field and not by adiabatic temperature variations, as in Dunlap's mechanism. The inertia and Stokes' drag of the droplets produce a phase shift between the velocities of the gas and the liquid droplets. This velocity difference in turn produces oscillations in the flux of fuel into the reaction zone and leads directly to a modulation of the heat release by the acoustic wave. The theoretical analysis predicts that, for droplet diameters between roughly 1 μm and 10 μm, the strength of the instability is proportional to the ratio of the viscous relaxation time of the drops, $\tau_{vis}$, to the transit time through the flame thickness, $\tau_t$. This mechanism leads to linear growth rates potentially much higher than those expected for gaseous mixtures. However, we will show here that, for Rayleigh's phase criterion to be satisfied, the frequency of the selected acoustic mode, $\omega$, must be higher than a critical value which is a fraction of the inverse of the transit time through the flame, $1/\tau_t$. The existence of a cut-off frequency, characteristic of sprays, is the signature of an internal relaxation phenomenon in the flame front. Our experiments show that it leads to a behaviour which is qualitatively different to that observed for gaseous combustion. One of the objectives of this paper is to observe these differences experimentally and to investigate the physical mechanisms responsible for the cut-off frequency.

The paper is organized as follows. Basic considerations concerning thermo-acoustic instabilities of flames are summarized in § 2. Section 3 describes the experimental set-up. Our experimental results are presented in § 4. A theoretical analysis of phenomena specific to sprays, in particular concerning the cut-off frequency, is presented in § 5. Our conclusions are presented in § 6. Details concerning the calculation of acoustic losses are presented in Appendix A, technical details concerning an extension of the calculation of Pelcé & Rochwerger are given in Appendix B. Calculations concerning the evaluation of the cut-off frequency with temperature-dependent diffusion coefficients are presented in Appendix C.

## 2. Background

### 2.1. *Phenomenology and orders of magnitude*

For quasi-homogeneous combustion in a cavity, the origin of thermo-acoustic instabilities is easily derived from the equation for acoustic wave propagation. To simplify the presentation, we consider the ideal case of a quasi-uniform non-dissipative medium, with flow velocities small compared to the speed of sound. These assumptions lead to the linear wave equation (see Clavin 1994 for a recent revue)

$$\frac{\partial^2 p}{\partial t^2} - c^2 \nabla^2 p = (\gamma - 1)\frac{\partial \dot{q}}{\partial t}, \tag{2.1}$$

where $p$ is the pressure, $c$ is the speed of sound, $\gamma = C_p/C_v$ the specific heat ratio and $\dot{q}(\boldsymbol{r}, t)$ the field of heat release rate per unit volume. If we write the feedback mechanism in a form in which the fluctuation $\delta\dot{q}$ is expressed as a linear function of $\delta p$, then (2.1), in a spatial Fourier representation, is seen to describe an acoustic oscillator which is amplified or damped, according to whether Rayleigh's criterion is satisfied or not. When the heat release rate fluctuations, $\delta\dot{q}$, and pressure fluctuations, $\delta p$, are in phase, the order of magnitude of the linear growth rate is proportional to

their ratio

$$\frac{1}{\tau_{ins}} \propto \frac{|\delta \dot{q}|}{|\delta p|}. \tag{2.2}$$

The case of a flame propagating in a tube differs from the preceding example in that it is an inhomogeneous problem. Typically, the flame front occupation ratio is smaller than, or of the order of, $\varnothing/L$, where $\varnothing$ is the tube diameter and $L$ the combustion chamber length. For high aspect ratios ($L/\varnothing \gg 1$), the reaction zone can be treated as a discontinuity on the scale of the longitudinal acoustic mode. The mass conservation relation for quasi-isobaric combustion can be written

$$\rho c^2 (\nabla \cdot \boldsymbol{u}) = \dot{q}, \tag{2.3}$$

where $\rho$ is the local gas density and $\boldsymbol{u}$ is the gas velocity. After spatial integration over the combustion zone, (2.3) leads to an expression for the jump in the fluctuations of gas velocity across the discontinuity:

$$(\delta u_b - \delta u_o) \frac{\pi \varnothing^2}{4} = \iiint \frac{1}{\rho c^2} \, \delta \dot{q} \, \mathrm{d}^3 r. \tag{2.4}$$

The subscripts $b$ and $o$ refer to the burnt and unburnt gas side respectively. Equation (2.4) expresses the gas expansion rate. The rate of change of the acoustic energy in the tube, $\varepsilon$, due to the combustion is given by the expression

$$\frac{\mathrm{d}\varepsilon}{\mathrm{d}t} = (\delta u_b - \delta u_o) \frac{\pi \varnothing^2}{4} \delta p \, . \tag{2.5}$$

Evaluating $\varepsilon$ in the form

$$\varepsilon \approx \left(\rho \, \delta u^2\right) \frac{\pi \varnothing^2}{4} L \approx \left(\frac{\delta u \, \delta p}{c}\right) \frac{\pi \varnothing^2}{4} L \approx \left(\frac{\delta u \, \delta p}{\omega}\right) \frac{\pi \varnothing^2}{4}, \tag{2.6}$$

where $\omega$ is the angular frequency of the acoustic mode, (2.5) and (2.6) enable us to evaluate the linear growth rate, $1/\tau_{inst}$, defined as

$$\frac{1}{\tau_{inst}} \equiv \frac{1}{\varepsilon} \frac{\mathrm{d}\varepsilon}{\mathrm{d}t} \approx \left(\frac{|\delta u_b - \delta u_o|}{|\delta u|}\right) \omega, \tag{2.7}$$

leading to the reduced growth rate

$$\frac{1}{\omega \tau_{ins}} \approx \left(\frac{|\delta u_b - \delta u_o|}{|\delta u|}\right). \tag{2.8}$$

Using (2.4) to evaluate the order of magnitude of the velocity jump fluctuation, we find, when the Rayleigh condition is satisfied

$$\frac{1}{\tau_{inst}} \approx \left(\frac{\Delta}{L}\right) \left(\frac{|\delta \dot{q}|}{|\delta p|}\right), \tag{2.9}$$

where $\Delta$ represents the thickness of the flame 'brush', $\Delta \lesssim \varnothing$. The coherence of this expression with the result obtained for the homogeneous case (2.2) is seen by noting that the heat release concerns only a fraction $\Delta/L$ of the total tube length.

### 2.2. *Transfer functions*

The transfer function characterizes the feedback mechanism of the acoustic wave on the flame front. For a pressure coupling, we define the transfer function, $Z$, in a

temporal Fourier representation, by

$$(\delta u_b - \delta u_o) \equiv Z \frac{\delta p}{\rho_o c_o}, \tag{2.10}$$

where $\delta u$ is positive towards the burnt gas, i.e. in the direction opposite to flame propagation. In the case of a planar flame, Clavin *et al.* (1990) give an analytical expression for $Z(\omega\tau_t)$ as a function of the acoustic frequency, $\omega$, reduced by the transit time through the laminar flame front, $\tau_t \equiv D_{th}/{U_L}^2$, where $D_{th}$ is the thermal diffusivity in the cold gas and $U_L$ is the laminar flame speed. This calculation was done for a simplified model in which the chemical reaction was reduced to a one-step reaction controlled by an Arrhenius law. The transfer function thus obtained is given by

$$Z = \frac{\beta}{2} M \frac{T_b}{T_o} (\gamma - 1) N(\omega\tau_t), \tag{2.11}$$

where $\beta$ is the reduced activation energy,

$$\beta = \frac{E}{RT_b} \frac{T_b - T_o}{T_b}, \tag{2.12}$$

$E$ is the activation energy, $R$ is the gas constant, $T_b$ and $T_o$ are the temperature of the burnt and unburnt gases, $M$ is the Mach number of the laminar flame speed, $M \equiv U_L/c_o$, and $N(\omega\tau_t)$ is a function of order unity depending on the inner structure of the flame, see figure 1. Equations (2.8) and (2.10) show that the transfer function is also the order of magnitude of the linear growth rate:

$$\frac{1}{\omega\tau_{inst}} \approx \frac{\beta}{2} M \frac{T_b}{T_o} (\gamma - 1). \tag{2.13}$$

The exact relation between the transfer function, $Z$, and the linear growth rate will be given later in (2.18). The presence of the activation energy, $\beta$, shows that the instability results from a feedback through the temperature fluctuation in the acoustic wave. The frequency dependence of $\mathrm{Re}(Z)$ is shown in figure 1 for different values of the Lewis number $Le \equiv D_{th}/D_m$, where $D_{th}$ and $D_m$ represent the thermal and mass diffusivities respectively. It can be seen in figure 1 that both the low and high frequency limits are independent of the details of the flame front structure. However this is not the case for the intermediate frequencies. The resonant behaviour seen for $\omega\tau_t \approx 1$ and $Le > 1$ is related to the existence of an intrinsic instability of the front at high Lewis numbers, described by a Hopf bifurcation (Sivashinsky 1977; Joulin & Clavin 1979). This instability is not observed in real premixed flames because the actual Lewis numbers are not sufficiently high.

In the case of a velocity coupling, we introduce a new transfer function, $Tr$, which is defined, in a temporal Fourier representation, by

$$(\delta u_b - \delta u_o) \equiv Tr\ \delta u_o. \tag{2.14}$$

Pelcé & Rochwerger (1992) have calculated this transfer function for the mechanism of modulation of the amplitude of cellular structures proposed by Rauschenbakh (1961). They consider a weakly cellular flame in the limit $ak \ll 1$, where $a$ is the amplitude of the cells and $k = 2\pi/\lambda$ is the wavenumber. Their results show that the transfer function scales as $(ak)^2$ times a function $P(\omega\tau_t, kd)$ of the reduced frequency, $\omega\tau_t$ and of the reduced wavenumber, $kd$, where $d \equiv D_{th}/U_L$ is the laminar flame

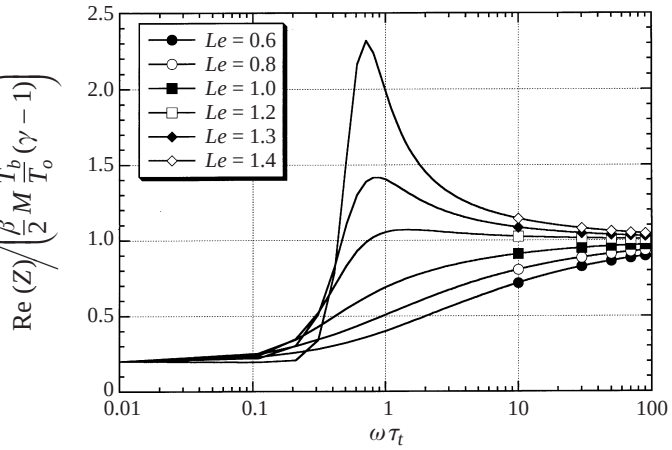


FIGURE 1. Normalized transfer function for the pressure coupling as a function of reduced frequency. Reduced activation energy $\beta = 20$, from Clavin *et al.* (1990).

thickness, see also Appendix B:

$$Tr = \frac{(ak)^2}{2}\left(\frac{T_b - T_o}{T_o}\right) P\,(\omega\tau_t, kd)\,. \tag{2.15}$$

The dependence of $\mathrm{Im}(Tr)$ on the reduced wavenumber, $kd$, is shown in figure 2($a$) for three different reduced frequencies, corresponding to the fundamental and first two harmonics of a 1.2 m tube. The transfer function is positive and decreases in magnitude with increasing frequency, except at very large wavenumbers. In our experiments, values of $kd$ are very small, $kd < 0.01$.

The velocity coupling proposed by Clavin & Sun (1991) for sprays or particle-laden gases, mentioned in the introduction, is of a different kind since it involves a modification of the internal structure of the flame and not a simple change of the geometry of the front. A discussion of some aspects of the transfer function for this mechanism will be presented in § 5. Here, we recall that the corresponding transfer function can be written

$$Tr = \frac{\beta}{2}\left(\frac{T_b - T_o}{T_o}\right)\frac{\tau_{vis}}{\tau_t} R\,(\omega\tau_t)\,,$$

where $\tau_{vis}$ is the viscous relaxation time of the droplet, given by Stoke's law (A 6) when the local Reynolds number is sufficiently small. $R(\omega\tau_t)$ is a function of order unity depending on the details of the inner structure of the flame. According to (2.8) and (2.14), the reduced linear growth rate is of the order of $\mathrm{Im}\,(Tr)$:

$$\frac{1}{\omega\tau_{inst}} \approx \mathrm{Im}\,(Tr) \approx \frac{\beta}{2}\left(\frac{T_b - T_o}{T_o}\right)\frac{\tau_{vis}}{\tau_t}. \tag{2.16}$$

A comparison of (2.3) and (2.16) shows that the coupling between acoustic waves and the inner structure of a flame is expected to yield a much stronger thermo-acoustic instability for sprays than for gases whenever

$$\frac{\tau_{vis}}{\tau_t} \gg (\gamma - 1)M.$$

This condition is fulfilled for droplets diameters greater than $\approx 1$ μm.

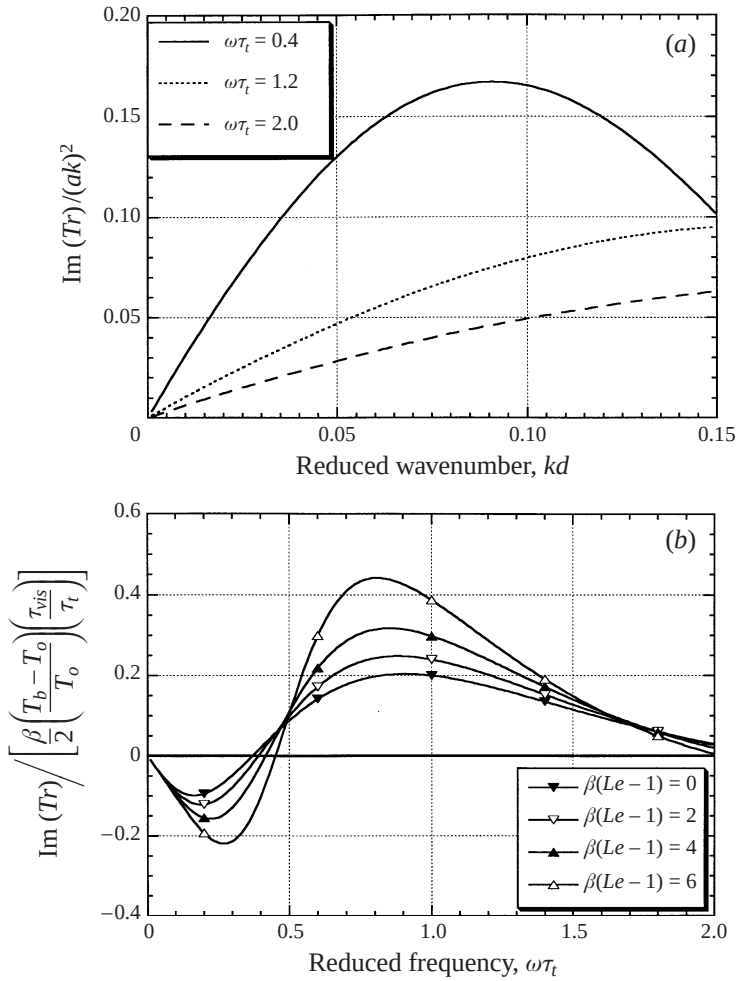


FIGURE 2. (*a*) Transfer function for the velocity coupling described by Pelcé & Rochwerger (1992). Markstein number = 4.5, other parameters are appropriated for a lean propane flame of burning speed 0.2 m s$^{-1}$. (*b*) Transfer function for the velocity coupling described by Clavin & Sun (1991). Parameters used are $\beta = 15$, $\ell^* = 0.026$ (dimensionless latent heat), $\xi_* = -4.2$ (dimensionless position of droplet vaporization zone), appropriate for the decane spray used in our experiments.

The typical frequency dependence of the reduced transfer function is shown in figure 2(*b*) for various values of $\beta(Le - 1)$, where $Le$ is the Lewis number. It can be seen that the transfer function changes sign at a frequency $\omega\tau_t \approx 0.4$.

### 2.3. *Gain calculation*

In the limit of high aspect ratio, the thickness of the combustion region is negligible compared to the acoustic wavelength. The longitudinal acoustic modes of the cavity can then be calculated using the transfer functions for the velocity jump at the interface and supposing continuity of the pressure (the pressure jump introduced by the combustion is of the order of $M^2$ and can be neglected here). The real and imaginary parts of the acoustic mode give the resonant frequency and the amplification (or damping) rate respectively. The calculation of the acoustic mode

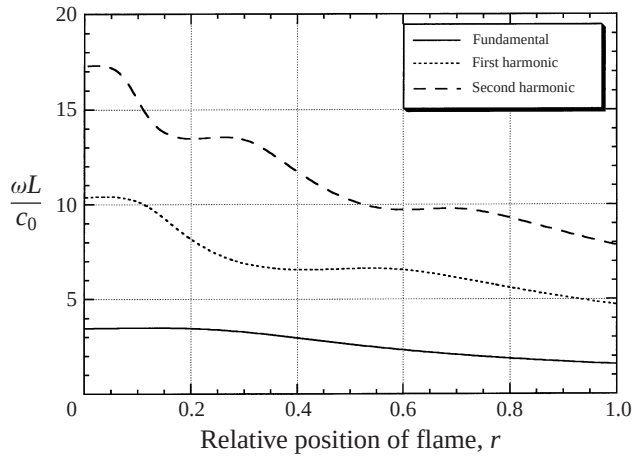


FIGURE 3. Dimensionless resonant frequencies of an open-closed cavity as a function of the relative position of the flame front in the tube for $T_b/T_o = 5$.

can be performed using a perturbation method when the module of the transfer function is small compared to 1. This is the case for the three mechanisms presented above when, respectively, the following inequalities are satisfied:

$$\frac{\beta}{2}\left(\frac{T_b}{T_o}\right) M \ll 1, \qquad (ak)^2 \ll 1, \qquad \frac{\beta}{2}\left(\frac{T_b - T_o}{T_o}\right)\frac{\tau_{vis}}{\tau_t} \ll 1.$$

To leading order, $\delta u_b = \delta u_o$ and the characteristic frequencies, $\omega$, of a tube open at one end, see Clavin *et al.* (1990), are given by the solutions of

$$\tan\left(r\frac{\omega L}{c_o}\right)\tan\left((1-r)\frac{c_o}{c_b}\frac{\omega L}{c_o}\right) = \frac{\rho_o c_o}{\rho_b c_b}, \tag{2.17}$$

where $r$ is the relative position of the flame front in the tube ($r \in [0,1]$) measured from the closed end ($r = 0$), $\omega L/c_o$ is the reduced frequency, $L$ is the length of the tube and $\rho$ the gas density. The dependence of the reduced frequency on the relative position of the front is shown in figure 3 for the first three acoustic modes.

The gain is calculated to first order in the perturbation introduced by the transfer function, see Clavin *et al.* (1990) and Pelcé & Rochwerger (1992). The linear growth rate of the instability, $1/\tau_{inst}$, for a pressure coupling is given by

$$\frac{L}{c_o\tau_{inst}} = \mathrm{Re}\,(Z)\,F\left(r, \frac{\omega L}{c_o}\right), \tag{2.18}$$

and for a velocity coupling by

$$\frac{L}{c_o\tau_{inst}} = \mathrm{Im}\,(Tr)\,G\left(r, \frac{\omega L}{c_o}\right), \tag{2.19}$$

the instability occurring when the right-hand side of (2.18) or (2.19) is positive. The structure functions, $F$ and $G$, are related only to the structure of the acoustic mode in the tube and are given by the following:

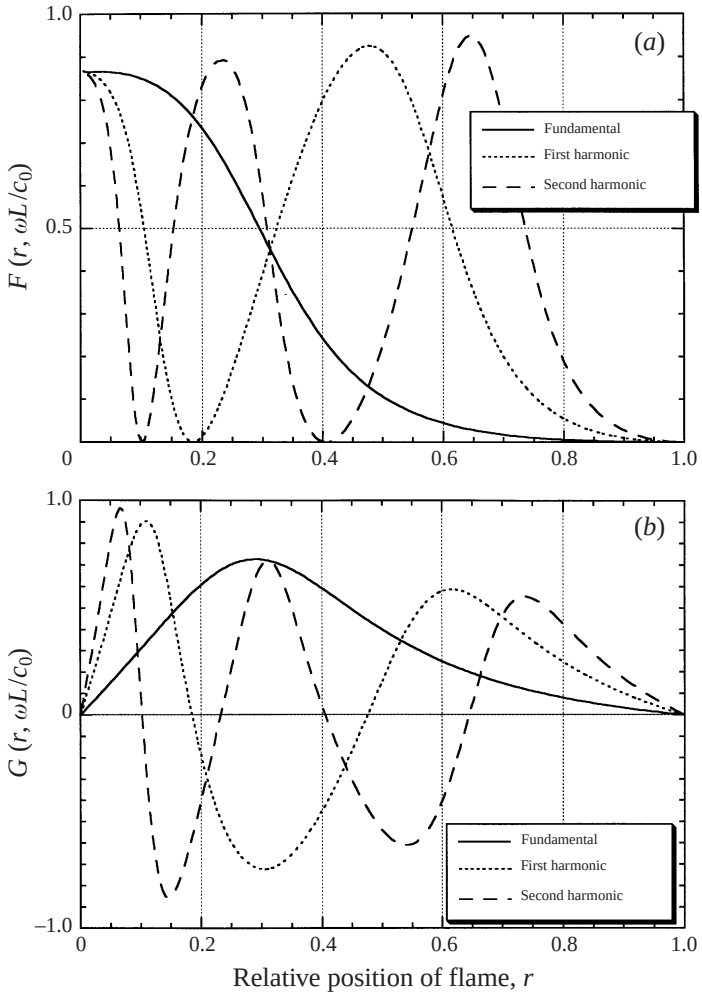


FIGURE 4. Acoustic structure functions for (*a*) pressure and (*b*) velocity coupling mechanisms, neglecting acoustic losses, $T_b/T_o = 5$.

$$F\left(r, \frac{\omega L}{c_o}\right) \equiv \frac{1}{r\left[1+\tan^2\left(r\frac{\omega L}{c_o}\right)\right] + \frac{\rho_b}{\rho_o}(1-r)\tan^2\left(r\frac{\omega L}{c_o}\right)\left[1+\tan^2\left((1-r)\frac{c_o}{c_b}\frac{\omega L}{c_o}\right)\right]}, \quad (2.20)$$

and

$$G\left(r, \frac{\omega L}{c_o}\right) \equiv \tan\left(r\frac{\omega L}{c_o}\right)\ F\left(r, \frac{\omega L}{c_o}\right), \quad (2.21)$$

in which $(\omega L)/c_o$ is given by the solutions of (2.17).

These characteristic structure functions are shown in figure 4 as a function of the position of the flame for the first three longitudinal acoustic modes. The structure function, $F$, for pressure coupling is always positive. Since the transfer function $\mathrm{Re}\,(Z)$ is also positive, see figure 2, the pressure mechanism is intrinsically unstable (but weak) at all frequencies and for all positions of the flame in the tube. The

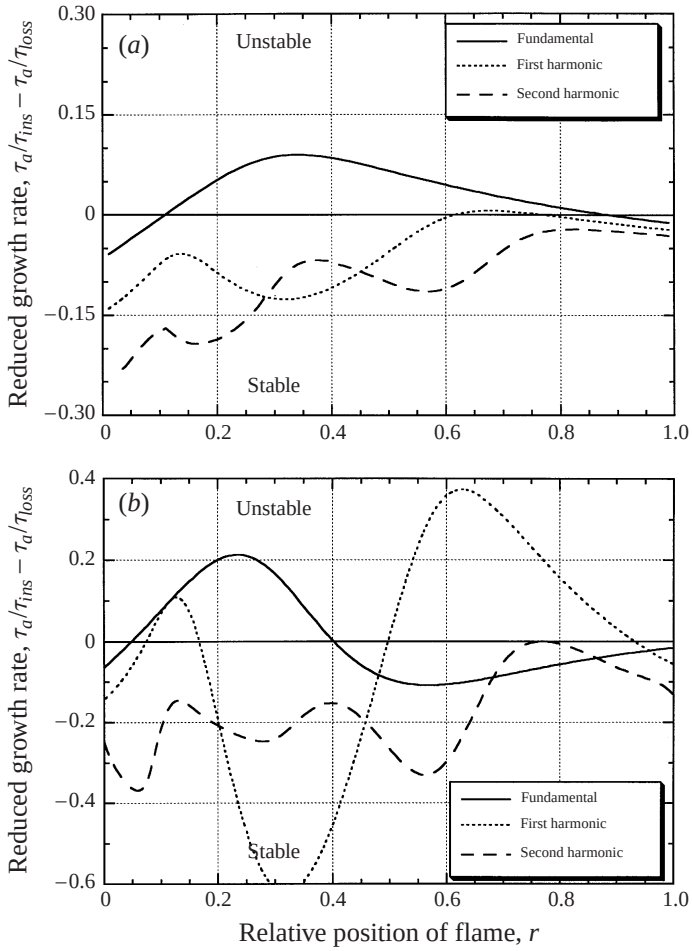


FIGURE 5. Calculated growth rates of instability, including acoustic losses for gaseous (*a*) and spray flames (*b*) (drop diameter 3.8 μm). Flame speed 20 cm $s^{-1}$.

structure function for velocity coupling, $G$, is positive for the fundamental frequency, but for higher harmonics it changes sign with position of the flame in the tube. The stability of the complete system then depends simultaneously on the sign of $G$ and the sign of the transfer function. We may thus expect a richer behaviour for velocity coupling, particularly in the case of a spray where the transfer function, $Tr$, also changes sign with frequency, see figure 2(*b*).

### 2.4. *Actual growth rate*

The experimentally observed growth rate results from the competition between the specific gain of the coupling mechanism, described by (2.18) and (2.19), and the acoustic losses of the combustion chamber. The acoustic damping has essentially three different origins, all of comparable strength in our experiments: radiative losses from the open end of the tube; wall losses associated with the thermal and viscous boundary layers; and, finally, dissipative losses due to the presence of droplets in the spray case. The corresponding damping rates are treated in detail, including the presence of a flame, in Appendix A. The experimental in-

stability appears when the gain produced by the flame is just greater than the acoustic losses of the tube. In the linear part of the growth, the specific gain and losses have similar order of magnitude. It is thus essential to have a good estimate of the total acoustic losses in the presence of flame. To illustrate the preceding paragraphs, we have calculated the global growth rate of the instability, including detailed acoustic losses, as a function of the position of the flame in the tube, for the fundamental mode and for the first two harmonics for the case of velocity coupling of a gaseous propane flame, corresponding to the transfer functions of figure 2(*a*), and for a spray of decane droplets corresponding to the transfer function of figure 2(*b*) with $\beta(Le-1)=6$. The acoustic losses are calculated following Appendix A for a tube 1.2 m long and 0.1 m diameter. The calculated growth rates are shown in figure 5. They are normalized by the characteristic acoustic time, $\tau_a \equiv L/c_o$. Note that the frequency is a function of the position of the flame, see figure 3.

For the case of a gaseous flame, only the fundamental mode is predicted to be unstable. At higher frequencies the acoustic losses dominate the instability, see figure 5(*a*). In the case of a spray flame, the growth rates are higher. The oscillations of the structure function, $G$, coupled with the change in sign of the transfer function leads to a rich behaviour. In the example shown in figure 5(*b*), the fundamental frequency is predicted to be unstable only in the lower half of the tube where the fundamental acoustic frequency is higher than the cut-off frequency in this 1.2 m tube. The most unstable frequency is initially the first harmonic and there is a small range of positions near the centre of the tube in which all harmonics are found to be stable. This predicted behaviour may be compared qualitatively with the observation presented in figure 9(*b*) for a flame of decane droplets. We will come back to these points in §§ 4 and 5.

## 3. Experimental set-up

The experimental apparatus is quite simple and is shown schematically in figure 6. The combustion chamber is a cylindrical Pyrex tube of length $L = 1.2$ m and diameter $\varnothing = 0.1$ m. The acoustic conditions are closed at the bottom and open at the top so that the frequencies of the longitudinal modes of a homogeneous case are given by $f_n = (2n+1)\,c/4L$, where $c$ is the speed of sound and $n$ the harmonic number. Without flame, the frequency of the fundamental mode, $f_0$, is $\approx 71$ Hz. When a flame front is present in the tube, the resonant frequencies are increased and depend on the relative position of the flame front in the tube, see figure 3. The frequencies of the radial and tangential modes, which scale as $c/\varnothing$, are very much higher and have not been observed.

Mixture ratios are controlled by sonic nozzles and the droplets were generated using a 'Sonicore' airblast atomizer. The mean diameter of the droplets and the diameter spread were obtained from an analysis of the intensity distribution in the Fraunhofer diffraction pattern of the spray. The diffraction pattern was calculated, assuming a log-normal distribution function for the droplet diameters, and fitted to the observed pattern. The best fit gave a Sauter mean diameter, $D_{32} = \langle D^3\rangle/\langle D^2\rangle = 3.8 \pm 0.5$ μm with a spread parameter of 1.47 μm. The variation of these values with the flows rates was small and within the quoted error over the range used in these experiments. According to the analysis of Bayvel & Jones (1981), for decane droplets whose refractive index is 1.41, the width of the diffraction pattern is given by Fraunhofer's expression to better than 20% for droplets of diameter greater than 1.5 μm, except for a narrow range of diameters between 2.50 and 2.68 μm. The droplet size distribution

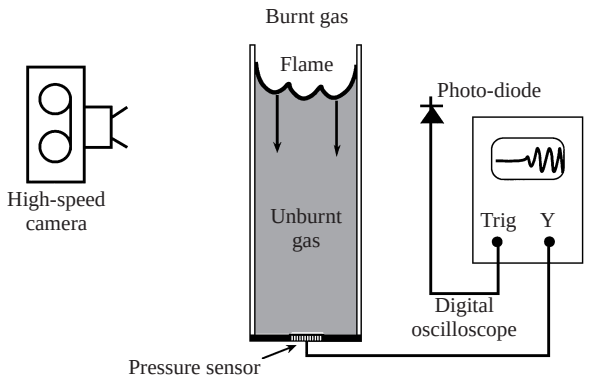


FIGURE 6. Schematic diagram of experimental apparatus.

from this generator has been checked independently using a Phase Doppler Particle Analyser. The values of $D_{32}$ from these two types of measurement differed by less than 7%. Neither method is capable of accurate measurement of droplet diameters less than 1 μm.

We used small droplets in order that the experimental conditions be situated in the domain of validity of the analytical study of Clavin & Sun. For small droplets, the vaporization time is given by the standard $D^2$ law (Law 1982; Williams 1985) which predicts a lifetime of 55 μs for 4 μm diameter decane droplets in a gaseous bath at 1000 K and 33 μs at 2000 K. The vaporization time is thus short, but not completely negligible compared to the transit time through the flame which varies with flame speed from 180 μs to 750 μs.

The mean distance between droplets lies between 0.5 and 1.0 times the flame thickness $d$, according to the equivalence ratio and resulting flame thickness. Since the Lewis number is close to unity, the time needed for fuel vapour to diffuse a distance equal to the mean droplet separation is a little less than the transit time in the flame. The flame structure is thus expected to contain a thin vaporization zone followed by a premixed gaseous flame front, see figure 16. However under these experimental conditions, we found that it was impossible to propagate a flame front in the spray, despite the fact that the global mixture ratio was within the flammability limits. To obtain flame propagation it was necessary to add a small amount of gaseous fuel (propane) to the mixture. In order to ensure spray flame propagation at all equivalence ratios used here, we added a constant background of propane with an equivalence ratio of 0.27. Moreover the vapour pressure of decane at room temperature is not negligible and the saturated vapour in air has an equivalence ratio of 0.13. In the following, the equivalence ratios stated for the sprays are global ratios comprising the sum of added gaseous propane (0.27), vaporized decane (0.13) and liquid decane (the rest). However, the purely gaseous part of the spray, with an equivalence ratio of 0.4, lies outside the flammability limits.

Concerning the effect of the presence of gaseous fuel on acoustic instability in spray combustion, we remark that all the fuel is vaporized in the preheat zone and burns in a premixed chemical reaction zone, see § 5. Thus the instability mechanism for gaseous combustion, described in Appendix B, can also lead to an instability in the spray case. Since only liquid fuel can participate in the spray instability mechanism, replacing liquid fuel by gaseous fuel will decrease the strength of the spray instability,

| | | |
|---|---|---|
| Geometrical characteristics | | |
| Tube length | $L$ | 1.2 m |
| Tube diameter | $\varnothing$ | 0.1 m |
| Gaseous mixture: propane–air | | |
| Thermal diffusivity | $D_{th}$ | $2.1\ 10^{-4}$ $m^2s^{-1}$ (in unburnt mixture) |
| Equivalence ratios | $\Phi$ | $0.7 < \Phi < 1.0$ |
| Laminar flame speeds | $U_L$ | $0.22 < U_L < 0.42$ m s$^{-1}$ |
| Burnt gas temperature | $T_b$ | $1880 < T_b < 2280$ K |
| Markstein number | Ma | 4.5 |
| Spray: decane–air | | |
| Thermal diffusivity | $D_{th}$ | $2.1\ 10^{-4}$ $m^2s^{-1}$ (in unburnt mixture) |
| Equivalence ratios | $\Phi$ | $0.73 < \Phi < 1.1$ (liquid + gaseous fuel) |
| Equivalence ratios | $\Phi$ | $0.33 < \Phi < 0.7$ (liquid fuel only) |
| Laminar flame speeds | $U_L$ | $0.20 < U_L < 0.38$ m s$^{-1}$ |
| Burnt gas temperature | $T_b$ | $1865 < T_b < 2260$ K |
| Droplet size | $D_{32}$ | 3.8 μm |
| Viscous relaxation time | $\tau_{vis}$ | 30 μs (see (A 6)) |
| Decane boiling point | | 447 K |
| Decane vaporization temperature | $T_*$ | $316 < T_* < 328$ K |
| Reduced vaporization position | $\xi_*$ | $-4.3 < \xi_* < -4.1$ |
| Reduced activation energy | $\beta$ | 15 |
| $\beta(Le-1)$ | | 6 |
| Reduced latent heat | $\ell_*$ | 0.026 (see Clavin & Sun 1991) |

TABLE 1. Values of experimental parameters.

but will have no effect on the contribution of the purely gaseous mechanism. It will be seen below that, for sprays, the proposed spray mechanism is totally dominant during onset of acoustic instability which occurs during the early stage of flame propagation in the tube, but that pressure peaks, characteristic of later stages of the gaseous mechanism, appear when the spray flame reaches the second half of the tube.

The burning velocities of the same sprays were obtained from an independent experiment by measuring the flame surface area in a laminar slot burner (Clanet 1995). The burning velocities were found to be of the order of 10% lower than those of a propane flame having the same total equivalence ratio. The values of the parameters used in these experiments and the following analysis are summarized in table 1. The vaporization temperature of the droplets is defined here as the equilibrium temperature at which the liquid has completely evaporated. Since the mass fraction of fuel is small, the vaporization temperature is considerably lower than the boiling point. The reduced latent heat is defined in Clavin & Sun (1991).

The tube is flushed and filled with the appropriate mixture through a stopcock at the bottom. The tube is then temporarily closed at both ends, for 1–2 min, until all gas motion has ceased. The sedimentation velocity of 4 μm droplets in air is calculated to be 350 μm s$^{-1}$. This velocity is less than the residual velocity of thermally induced convection currents in the quiescent mixture and no significant stratification or sedimentation was observed during the time that the gas flow was allowed to settle. The mixture is ignited at the open end where, according to the Rayleigh criterion, the presence of a pressure node, $\delta p = 0$, initially prevents any acoustic instability from occurring. The instability then develops as the flame propagates downwards.

The aim of this study is to determine which of the different theoretical mechanisms best describes the experimental observations. To compare with theories, we have measured the growth rate of the instability and the flame position at the onset of the instability. The acoustic pressure was measured using a piezo-electric sensor at the base of the tube, a numerical oscilloscope and a microcomputer for data analysis. The bandwidth of the pressure sensor and amplifier was 1 Hz–100 KHz. The signal was digitized with 4096 points without filtering. A spectrum analyzer was used to measure the acoustic losses of the combustion chamber. The flame position and shape were measured using a gated CCD video camera and also a high-speed film camera coupled to a pulsed copper vapour laser run at 3000 pulses $s^{-1}$.

## 4. Experimental results

### 4.1. *Qualitative observations*

The existence of an effect specific to the presence of spray combustion will be demonstrated by comparison with the case of gaseous combustion. In a tube 1.2 m long we have observed the following behaviour as a function of the global equivalence ratio, $\Phi$.

#### 4.1.1. *Gaseous combustion*

For $\Phi < 0.7$, no sound is produced during the flame propagation. The flame front has a cellular structure, containing one or more large cells. Figure 19 shows typical structures. The total flame area is about twice the cross-section of the tube and the flame propagates steadily downwards at about twice the laminar flame velocity, as would be expected.

For $0.7 < \Phi < 0.75$, in the upper half of the tube the flame is cellular but silent, as above. The fundamental acoustic mode becomes unstable when the flame is in the lower half of the tube. The acoustic level increases first exponentially, but rapidly saturates. During the period of saturation, the peak acoustic pressure, measured at the base of the tube, is between 0.005 and 0.01 bar. In the saturated state of this primary instability, the flame is quasi-planar and propagates at the laminar flame speed. The resonant frequency of the tube is a function of the relative lengths of the regions filled with cold and hot gas, see figure 3. For the 1.2 m tube, the acoustic frequency at the onset of instability was typically 120 Hz.

For $\Phi > 0.75$, in the upper half of the tube the flame is cellular but always silent, as above. The fundamental acoustic mode is unstable when the flame is in the lower half of the tube. The acoustic signal presents two distinct regions: the first corresponds to the primary instability, described above; the second, in which very high acoustic levels (up to $\pm 0.2$ bar) are reached, corresponds to the parametric instability studied by Searby & Rochwerger (1991). During the parametric instability, the flame has deep cellular structures, oscillating at half the acoustic frequency. These structures greatly increase the mean flame surface area. The flame can propagate ten to twenty times faster than the laminar flame speed. Close to stoichiometry, the transition from primary to secondary instability is rapid and continuous. In all cases, only the fundamental mode of the tube is observed. Typical pressure records and flame images can be found in Searby (1992).

#### 4.1.2. *Spray combustion*

For $0.65 < \Phi < 0.75$, the fundamental acoustic mode becomes unstable in the upper third of the tube and persists until the end. The acoustic level increases exponentially

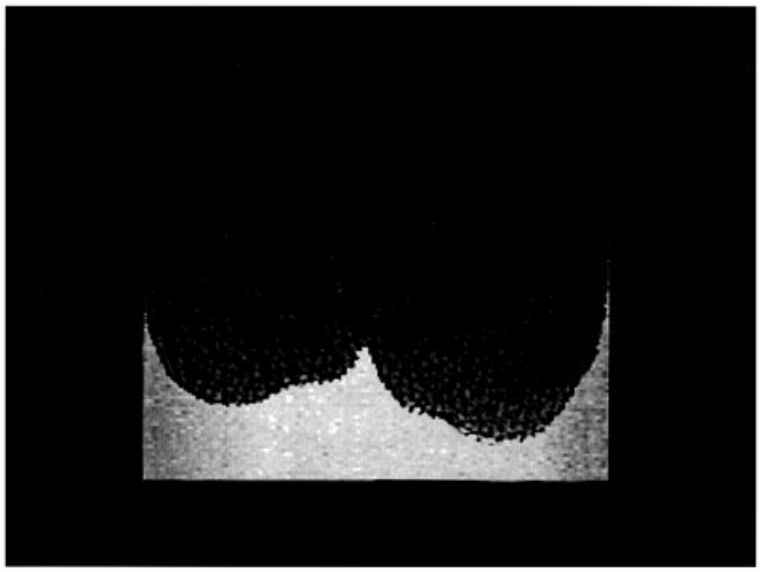

FIGURE 7. Tomographic cut through a cellular premixed spray flame at the onset of acoustic instability. Global equivalence ratio = 0.71, $U_L = 0.18\ \mathrm{m\,s^{-1}}$.

at first and then rapidly saturates. The saturated acoustic level, measured at the base of the tube, increases gradually from about 0.01 bar to 0.025 bar as the flame descends the tube. This level is higher than the corresponding gaseous case. Before the onset of instability, the flame front has large cellular structures very similar to those of the gaseous case, see figure 7. During the instability, the flame generally shows small-amplitude small-scale cells oscillating at half the acoustic frequency, similar to those observed at the onset of the parametric instability in the gaseous case. However the amplitude of these structures remains small and the flame front continues to propagate at about twice the laminar flame speed. This behaviour is shown in figure 8(*a*). The acoustic frequency at the onset of instability is typically 85 Hz.

For $0.75 < \Phi < 0.95$, the first harmonic (typically 240 Hz) becomes unstable in the upper third of the tube and the fundamental mode appears later in the propagation. The transition between the two modes is made through a silent zone, the length of which depends on the equivalence ratio (figures 8 and 9). In some cases the length of this silent zone reduces to zero. The amplitude of the first harmonic increases first exponentially and rapidly saturates to a peak level between 0.01 and 0.02 bar. During this saturated state, the flame again has small-amplitude oscillating cells and continues to propagate at about twice the laminar flame speed. Some time after the transition to the fundamental frequency of the tube, the acoustic level increases very rapidly to a much higher level, between 0.1 and 0.25 bar, with deep oscillating cells. This secondary instability has the same characteristics as the parametric instability described previously for gaseous flames. We will not be concerned with this effect here.

For $0.95 < \Phi < 1.1$, the acoustic signal contains, successively, three different frequencies. The second harmonic of the tube, at $\approx 400$ Hz, is unstable very early in the propagation and then transits to the first harmonic, at $\approx 260$ Hz, which itself transits to the fundamental mode in the lower third of the tube. Such behaviour is

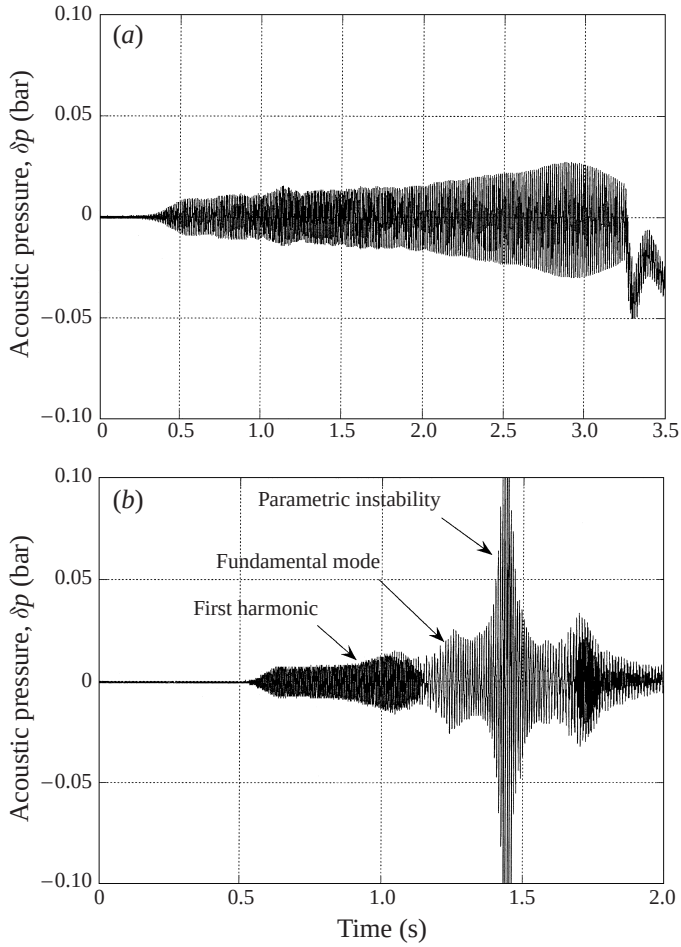


FIGURE 8. Record of the acoustic pressure for spray flame (decane), in a 1.2 m tube: (*a*) equivalence ratio = 0.7, laminar flame speed = 0.17 m $s^{-1}$; (*b*) equivalence ratio = 0.8, laminar flame speed = 0.23 m $s^{-1}$. The instability changes frequency at time = 1.15 s.

shown in figure 9(*b*). The first and second harmonics saturate at a peak level around 0.25 bar. The parametric instability is triggered shortly after the transition to the fundamental frequency; however there is no clear discontinuity between the end of the primary acoustic instability at the fundamental frequency and the onset of the secondary parametric instability. During the saturated states the flame propagates at two to three times the laminar flame speed. During the parametric instability the flame propagates at ten to twenty times the laminar flame speed.

The different positions in the tube for which the various harmonics are unstable are shown as a function of the equivalence ratio in figure 10 for gaseous and spray combustion respectively. Other tubes with various lengths have been used; the behaviour is qualitatively similar, only the limiting values of the equivalence ratio for the change of regime are modified. In the case of spray combustion, increasing the length of the tube for a given equivalence ratio also increases the harmonic number of the first unstable frequency. For example in a tube 5 m long, the first unstable frequency was the 9th harmonic. This was never observed with gaseous combustion for which the unstable frequency was always the fundamental for all tube lengths. In

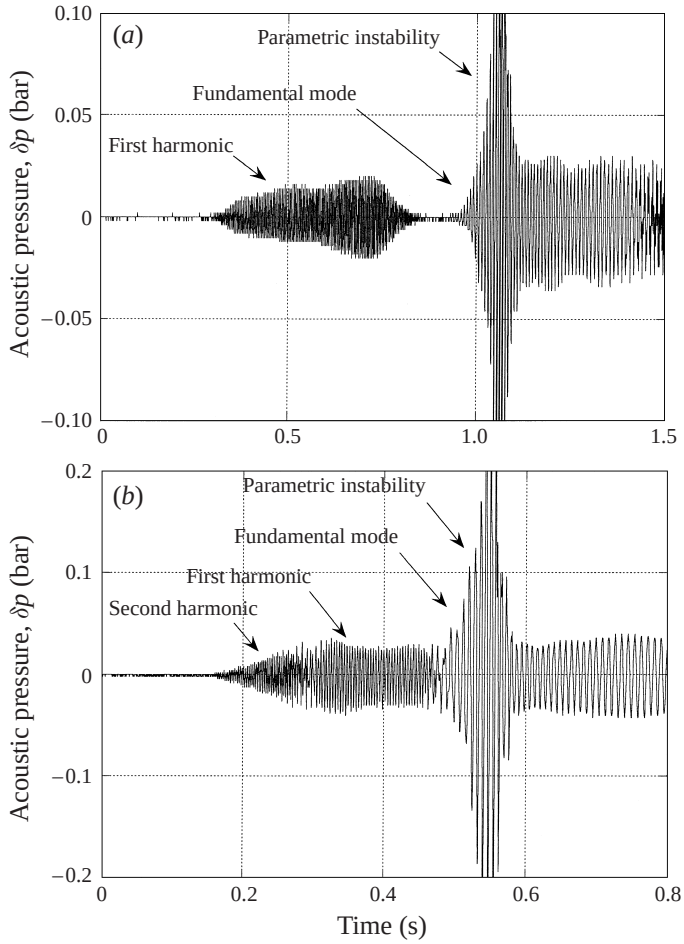


FIGURE 9. Record of the acoustic pressure for spray flame (decane), in a 1.2 m tube. (*a*) Equivalence ratio = 0.9, laminar flame speed = 0.3 m $s^{-1}$. There is a period of silence between the change of frequency. (*b*) Equivalence ratio= 1.1, laminar flame speed = 0.36 m $s^{-1}$. The instability appears successively at three different frequencies.

the following sections we will be concerned only with the initial exponential part of the growth of the primary acoustic instability and the position in the tube at which it occurs.

### 4.2. *Comparison of measured and calculated growth rates*

In this section, we present the experimental data for growth rates both in dimensional units (tables 2 and 3) and in a form suitable for comparison with the theoretical values, calculated for the different mechanisms presented in § 2.

As already mentioned, thermo-acoustic instabilities result from a coupling between the acoustic modes, which depend on the geometry of the combustion chamber, and the heat release rate, which is a function of the internal structure of the front and of the total surface area of the flame. The experimental parameters controlling the instability are: the length of the tube, which imposes the available acoustic frequencies; and the equivalence ratio of the mixture which governs the mean local heat release rate. The shape of the flame front is a free parameter. The growth rate of the instability will be

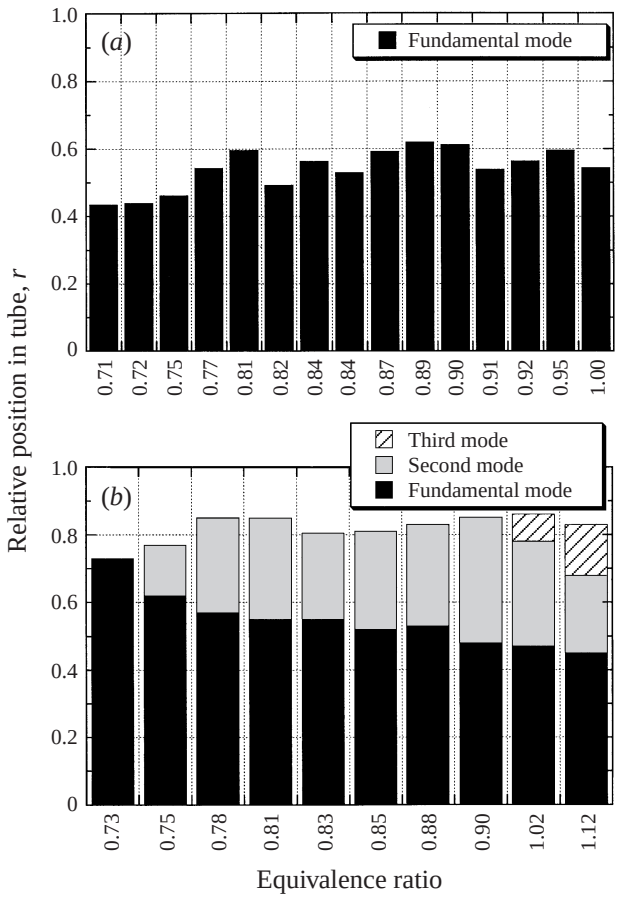


FIGURE 10. Regions of acoustic instability for gaseous flame (*a*) and spray flame (*b*). The bar marks the position in the tube at which the acoustic instability first occurs. The flame propagates from the open end ($r = 1$) to the closed end ($r = 0$). The cross-hatching indicates the frequency. For the spray flame, higher harmonics are excited in the upper region of the tube as the flame speed is increased.

presented as a function of the dimensionless frequency, $\omega\tau_t$ where $\omega$ is the angular acoustic frequency and $\tau_t$ the transit time in the flame front, defined by $\tau_t \equiv D_{th}/U_L^2$. The dimensionless parameter, $\omega\tau_t$, can be changed in discrete steps by changing the length of the tube, $L$. It can also be varied continuously by changing the flame speed, $U_L$. In practice we use the latter.

The growth rates for various experimental conditions were obtained from analysis of the exponential part of the primary acoustic instability using high-resolution recordings such as shown in figure 11. Only the exponential part of the signal was retained for analysis. There was no difficulty in discriminating this region from the region affected by saturation. These *observed* growth rates, $\tau_{obs}^{-1}$, were then corrected for acoustic losses, $\tau_{loss}^{-1}$, see Appendix A, calculated for the observed position of the flame in the tube, to obtain the *experimental* linear growth rate, $\tau_{exp}^{-1} \equiv \tau_{obs}^{-1} + \tau_{loss}^{-1}$ that would be measured in the absence of acoustic losses. The numerical values are given in tables 2 and 3 along with the flame speed, the frequency and the position in the tube at which the instability first occurred.

In the following we will present the ratio of the experimental growth rate, $\tau_{exp}^{-1}$, to

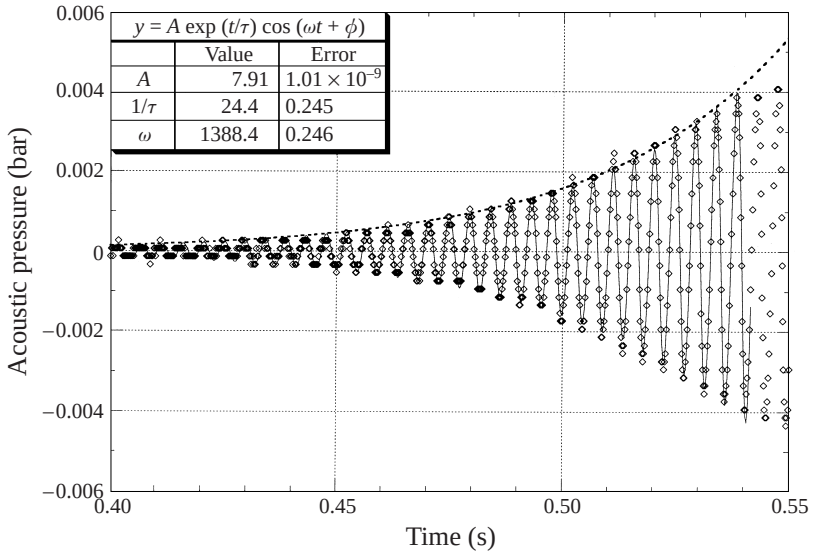


FIGURE 11. Detail of early stage of acoustic instability showing measured acoustic pressure (symbols) and fitted exponential-cosine function (continuous line). The dotted line is the envelope of the fitted exponential growth. The onset of saturation is apparent at 0.54 s. Decane–air spray flame. Equivalence ratio = 0.75, laminar flame speed = 0.2 m $s^{-1}$.

| $\phi$ | $U_L$ (m $s^{-1}$) | $r$ | $f$ (Hz) | $1/\tau_{obs}$ ($s^{-1}$) | $1/\tau_{loss}$ ($s^{-1}$) | $1/\tau_{exp}$ ($s^{-1}$) |
|---|---|---|---|---|---|---|
| 0.71 | 0.23 | 0.44 | 127.3 | 2.8 | 4.4 | 7.2 |
| 0.72 | 0.24 | 0.44 | 126.8 | 4.5 | 4.3 | 8.8 |
| 0.75 | 0.26 | 0.46 | 123.5 | 3.7 | 4.1 | 7.8 |
| 0.77 | 0.28 | 0.54 | 112.0 | 4.7 | 3.3 | 8.0 |
| 0.80 | 0.30 | 0.59 | 105.0 | 7.7 | 3.0 | 10.7 |
| 0.82 | 0.31 | 0.49 | 119.0 | 8.6 | 3.7 | 12.3 |
| 0.84 | 0.33 | 0.56 | 109.3 | 13.6 | 3.2 | 16.8 |
| 0.84 | 0.33 | 0.53 | 113.7 | 11.3 | 3.4 | 14.7 |
| 0.87 | 0.35 | 0.59 | 105.5 | 12.7 | 3.0 | 15.7 |
| 0.89 | 0.36 | 0.62 | 102.3 | 7.3 | 2.9 | 10.2 |
| 0.90 | 0.37 | 0.61 | 103.2 | 11.9 | 2.9 | 14.8 |
| 0.91 | 0.38 | 0.54 | 112.4 | 18.7 | 3.4 | 22.1 |
| 0.92 | 0.38 | 0.56 | 109.2 | 12.3 | 3.2 | 15.5 |
| 0.95 | 0.40 | 0.59 | 105.0 | 16.3 | 3.0 | 19.3 |
| 1.00 | 0.42 | 0.54 | 111.7 | 20.7 | 3.3 | 24.0 |

TABLE 2. Observed growth rate, acoustic losses and total experimental growth rate of acoustic instability for propane–air flames, $L = 1.22$ m, $\varnothing = 10$ cm.

the calculated growth rate, $\tau_{inst}^{-1}$, for the various coupling mechanisms, see equations (2.18) and (2.19), as a function of the reduced frequency, $\omega\tau_t$. The structure functions $F$ and $G$ are computed from equations (2.17), (2.20) and (2.21).

4.2.1. *Comparison for direct coupling with pressure and temperature field*

The comparison with the pressure coupling described by Clavin *et al.* (1990) is shown in figure 12. The theoretical growth rate for this mechanism, used here as

| $\phi$ | $U_L$ (m s$^{-1}$) | $r$ | $f$ (Hz) | $1/\tau_{obs}$ (s$^{-1}$) | $1/\tau_{loss}$ (s$^{-1}$) | $1/\tau_{exp}$ (s$^{-1}$) |
|---|---|---|---|---|---|---|
| 0.70 | 0.17 | 0.80 | 84.5 | 13.3 | 5.0 | 18.3 |
| 0.70 | 0.17 | 0.79 | 84.8 | 13.3 | 5.0 | 18.3 |
| 0.70 | 0.17 | 0.80 | 84.5 | 14.3 | 5.0 | 19.3 |
| 0.71 | 0.18 | 0.78 | 86.1 | 15.1 | 5.2 | 20.3 |
| 0.71 | 0.18 | 0.76 | 87.8 | 17.7 | 5.3 | 23.0 |
| 0.74 | 0.19 | 0.73 | 268.6 | 14.7 | 13.2 | 27.9 |
| 0.75 | 0.20 | 0.81 | 221.0 | 24.4 | 11.0 | 35.4 |
| 0.76 | 0.21 | 0.86 | 239.4 | 27.8 | 11.0 | 38.8 |
| 0.79 | 0.23 | 0.88 | 233.5 | 26.8 | 11.0 | 37.8 |
| 0.81 | 0.25 | 0.87 | 237.0 | 29.8 | 11.6 | 41.4 |
| 0.84 | 0.27 | 0.88 | 234.8 | 27.0 | 11.7 | 38.7 |
| 0.86 | 0.29 | 0.89 | 232.0 | 26.0 | 11.9 | 37.9 |
| 0.89 | 0.30 | 0.88 | 234.1 | 27.7 | 12.3 | 40.0 |
| 0.93 | 0.34 | 0.88 | 235.1 | 28.2 | 13.0 | 41.2 |
| 0.95 | 0.35 | 0.88 | 424.5 | 26.5 | 30.8 | 57.3 |
| 1.03 | 0.38 | 0.91 | 415.1 | 35.6 | 31.2 | 66.8 |
| 1.14 | 0.35 | 0.87 | 427.4 | 30.0 | 37.0 | 67.0 |

TABLE 3. Observed growth rate, acoustic losses and total experimental growth rate of acoustic instability for decane–air spray flames, $L = 1.22$ m, $\varnothing = 10$ cm.

a reference, was calculated using a reduced activation energy $\beta = 10 \pm 2.5$ and $\beta(Le - 1) = 4$. The sensitivity of the theoretical growth rate to these parameters is not strong. The burnt gas temperatures and density were calculated numerically using data from the SANDIA CHEMKIN package, Kee, Miller & Jefferson (1980), Kee, Rupley & Miller (1990), assuming equilibrium chemistry for propane–air flames. Laminar flame speeds were taken from Yamaoka & Tsuji (1984). It can be seen that the experimentally observed growth rates, corrected for acoustic losses from the tube, are two to three orders of magnitude higher than the growth rates calculated for this mechanism. This is equally true for both gaseous and for spray combustion. Moreover, it can also be seen that the growth rates in the spray are, in general, an order of magnitude greater than the gaseous growth rates. We conclude that the direct coupling between the combustion rate and the pressure or temperature fluctuations in the acoustic wave, first proposed by Dunlap, is certainly not the mechanism responsible for the observed instability.

4.2.2. *Comparison for coupling with the acceleration field: cellular flames*

Pelcé & Rochwerger (1992) have calculated the growth rate of the acoustic instability driven by the effect of the acoustic acceleration on the geometry of the flame front. They have treated the case of a weakly cellular planar flame propagating downwards at the threshold of the planar flame instability where the value of the marginally unstable wavenumber is a simple function of the Markstein and Froude numbers (Pelcé & Clavin 1982; Searby & Quinard 1990), leading to a simplification of the dispersion relation between complex frequency and wavenumber. Experimentally we find that such a weakly cellular flame (equivalence ratio $\approx 0.55$) is acoustically stable. The acoustic instability occurs only for faster flames which have strong nonlinear cells whose size is much greater than that of the most unstable wavelength predicted by linear theory.

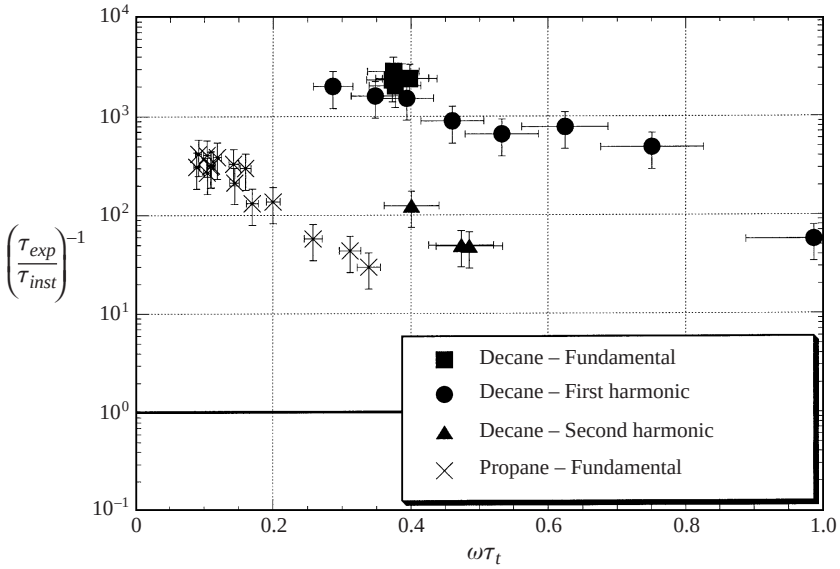


FIGURE 12. Ratio of the experimentally measured growth rates of the acoustic instability to the predicted growth rate for the one-dimensional mechanism of pressure coupling between the combustion rate and the acoustic wave. The error bars represent 25% incertitude in $\beta$, plus errors in determination of $\tau_{exp}^{-1}$.

We have extended and extrapolated the work of Pelcé & Rochwerger in order to apply their linear analysis for weak cells to our experimental configuration of nonlinear cells far from the threshold of the planar flame instability. The technical details are given in Appendix B. Although this extended theory is not strictly valid for the amplitude of the cells observed in our experiments, we still expect the calculation to give the correct order of magnitude for the growth rate of the instability associated with this mechanism.

The ratio of the experimentally measured growth rates to the calculated growth rates for this mechanism is shown in figure 13. For gaseous combustion, this ratio is close to unity and we conclude that this model provides a satisfactory explanation of our experimental gas-phase results, despite the fact that we have compared the results of a small-amplitude theory with observations on large-amplitude cells. This mechanism is probably the one which is responsible for the primary acoustic instability in gaseous combustion. However, for spray combustion, the experimentally measured growth rates are more than an order of magnitude higher than predicted by this mechanism and the comparison is not satisfactory.

4.2.3. *Comparison for coupling with the acceleration field: spray flames*

Figure 14 shows the comparison of our experimental results with the predictions of Clavin & Sun for the spray coupling mechanism. Since both the transfer function, $Tr$, and the acoustic structure function, $G$, for this mechanism are expected to change sign, we compare the experimental and theoretical values of the reduced transfer function, rather than the ratio of measured to calculated growth rates. The experimentally measured growth rates were corrected for acoustic losses, including the losses associated with the presence of droplets, see table 3. They were then normalized by the characteristic acoustic time scale, $L/c_o$ (see (2.19)) and finally reduced by the value of the acoustic structure function, $G$ (see (2.21)), calculated for the position in

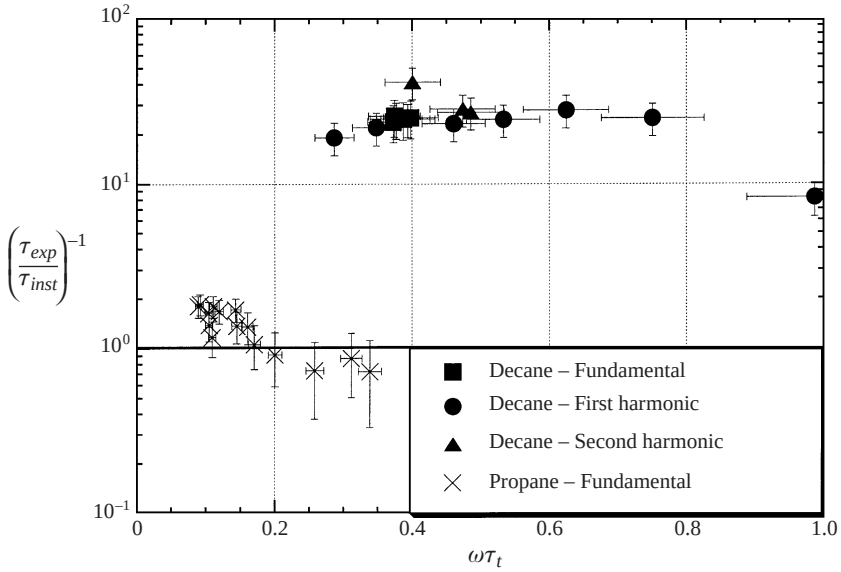


FIGURE 13. Ratio of the measured growth rates of the acoustic instability and the predicted growth rate for the two-dimensional mechanism of coupling between the acoustic acceleration and the amplitude of spontaneous cellular structures. The error bars represent 10% incertitude in measurement of the aspect ratio of the cells, plus errors in determination of $\tau_{exp}^{-1}$.

the tube at which the acoustic instability first occurs. This experimentally determined transfer function was then further reduced by 0.5 $\beta$ $(\tau_{vis}/\tau_t)(T_b - T_o)/T_o$, where we have taken $\beta$=15. $T_b$ was assumed equal to the value of a propane flame having the same flame speed, the viscous relaxation time of the droplets, $\tau_{vis}$, was calculated from (A 6) for 3.8 μm diameter droplets and $\tau_t \equiv D_{th}/U_L^2$ was calculated from the measured spray flame speeds. The theoretical transfer function was calculated using parameter values given in the caption to figure 14.

It can be seen that the experimentally determined values of the transfer function for this mechanism are of the same order of magnitude as the theoretical values. However the experimental points do not lie exactly on the theoretical curve, but seem to be shifted towards smaller values of reduced frequency, $\omega\tau_t$. Moreover the values obtained when different harmonic frequencies of the tube appeared do not lie exactly on the same curve. The theoretical transfer function is negative for values of $\omega\tau_t$ less than 0.45, indicating that the system should be unstable only for $\omega\tau_t > 0.45$. The experimental points show that the system is actually unstable for $\omega\tau_t > 0.3$. However no instability was ever observed for reduced frequencies smaller than this value. If the tube length was increased and/or the flame speed increased so as to lower the value of $\omega\tau_t$, it was found that the instability always occurred on a harmonic frequency of the tube such that $\omega\tau_t > 0.3$, indicating the existence of a cut-off at this frequency. As already mentioned in § 4.1.2, the first unstable frequency in a 5 m tube was the 9th harmonic.

This change in harmonic number with change in laminar flame speed is presented more clearly in figure 15 using non-dimensional coordinates. In this figure the horizontal axis represents the transit time of the flame, $\tau_t \equiv D_{th}/U_L^2$, reduced by a characteristic acoustic time scale of the chamber, $\tau_a \equiv L/c_0$. This ratio $\tau_t/\tau_a$ varies as the inverse of the square of the laminar flame speed. The vertical axis represents the

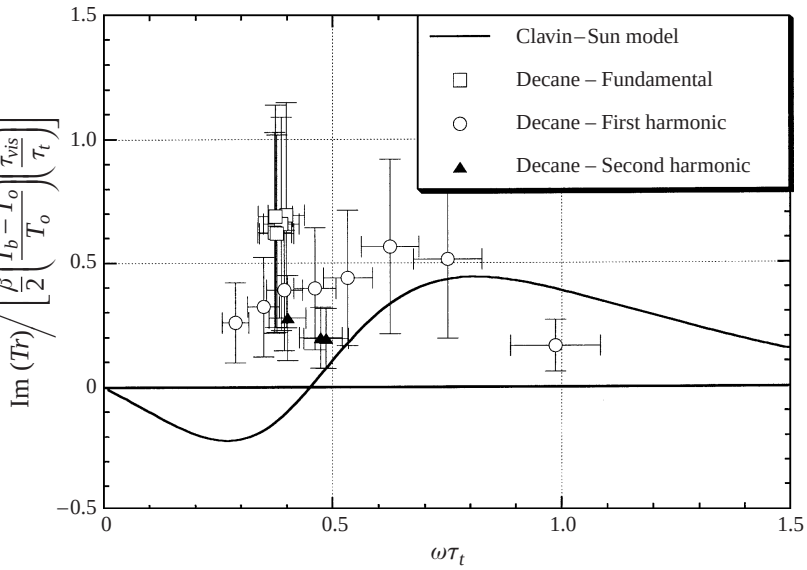


FIGURE 14. Comparison of theoretical transfer function for the spray mechanism of Clavin & Sun and the transfer function deduced from the experimentally measured growth rates of the acoustic instability of the decane spray. The theoretical curve was calculated using the following values (see table 1) : $\beta = 15$, $\beta(Le - 1) = 6$, dimensionless position of vaporization zone, $\chi_* = -4.2$, dimensionless latent heat, $\ell^* = 0.026$. The experimental results were reduced using a viscous relaxation time, $\tau_{vis} = 30$ μs for droplets 3.8 μm diameter.

angular frequency of the *first* unstable mode, $\omega$, reduced by the flame transit time $\tau_t$. The acoustic time of the chamber is fixed by the length of the tube and the acoustic frequency of the instability depends on the harmonic number that is chosen by the system. In our experiment, the transit time of the flame is decreased by increasing the laminar flame speed. For the gaseous case (propane/air), the instability always occurs at the fundamental frequency of the tube for all flame speeds. The locus of $\omega\tau_t$ for the propane flame thus decreases monotonically towards zero as the flame speed is increased. No sound is emitted for slow flames such that $\tau_t/\tau_a > 0.11$ in this 1.2 m tube. However, in the case of spray combustion the fundamental mode of the tube is excited initially only for slow flames ($\tau_t/\tau_a > 0.15$) whose transit time is such that $\omega\tau_t > 0.3$. As the flame speed is increased, $\omega\tau_t$ decreases until it reaches a limiting value close to 0.3. When the flame speed is further increased ($\tau_t/\tau_a < 0.15$), the first overtone of the chamber is excited instead of the fundamental frequency and thus $\omega\tau_t$ jumps to a higher value. As the flame speed is further increased, the value of $\omega\tau_t$ decreases until the limiting value of 0.3 is again reached ($\tau_t/\tau_a = 0.05$). At this stage a further increase in the flame speed ($\tau_t/\tau_a < 0.05$) causes the second overtone of the chamber to be excited, with a corresponding upward jump in the value of $\omega\tau_t$.

The fixed value, $\omega\tau_t = 0.3$, of the reduced cut-off frequency observed in our experiments for flames of different equivalence ratio in different tubes, is the signature of a relaxation mechanism involving unsteady effects of the internal structure of the flame. In order to explain this fixed cut-off frequency, the theoretical analysis initiated by Clavin & Sun (1991) is revisited in the following section.

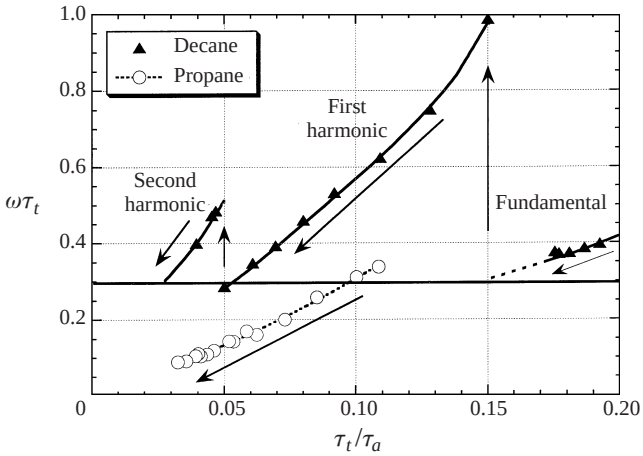


FIGURE 15. Evolution of the reduced frequency, $\omega\tau_t$, of the acoustic instability as the flame transit time is decreased for gaseous and spray combustion. The arrows indicate the direction of decreasing transit time (increasing flame speed). $\tau_a \equiv L/c_o$, $\tau_t \equiv D_{th}(T_o)/U_L^2$.

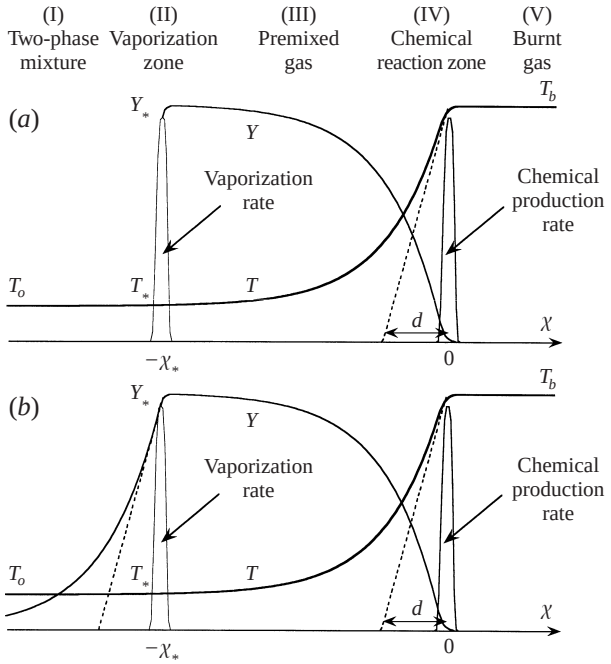


FIGURE 16. Model structure of the spray flame. $T$ is the temperature and $Y$ the mass fraction of gaseous fuel. The structure is dived into five zones: (I) upstream zone of unburnt spray, (II) a thin vaporization zone, (III) a gaseous premixed zone, (IV) a thin chemical reaction zone, (V) downstream zone of burnt gas. (*a*) Thermal equilibrium model of vaporization. (*b*) Non-equilibrium model of vaporization.

## 5. Velocity coupling in spray combustion

We will limit our discussion to the analysis of a model of minimal complexity, but sufficient to show the origin of the change of sign of the transfer function and to compute the cut-off frequency with a good approximation.

### 5.1. *Flame models and qualitative analysis*

We consider a fuel-lean mixture of fuel droplets, whose radius, $r_d$, is sufficiently small for the vaporization time to be negligible compared to the transit time, $\tau_t$, of the fluid through the flame thickness. The liquid fuel is then fully vaporized before burning. This is typically the case at atmospheric pressure for droplets whose radius is less than a few microns. Tomographic cuts of our flames show that the droplets disappear completely before entering the luminous reaction zone and so the structure of our flames is in satisfactory agreement with this hypothesis. We use the simplest model of gas-phase combustion (Zeldovich & Frank-Kamenetskii 1938), in which the reactants are transformed to burnt products in a single-step exothermic reaction, characterized by an activation energy large enough to confine the reaction zone to a thin sheet at high temperature close to $T_b$ (flame temperature). We will also assume that the temperature at which liquid droplets can be fully vaporized, $T_*$, is much lower than $T_b$. Typically, at ordinary conditions, $T_* \approx 400$ K, and $T_b \approx 2500$ K. We will see later that the cut-off frequency, $\omega_*$, is of the order of the inverse of the time, $\tau_*$, taken for a fluid particle to travel from the isotherm $T_*$ to the isotherm $T_b$

$$\omega_* \tau_* = O(1). \tag{5.1}$$

The theoretical analysis is greatly simplified by the assumption that $T_*$ is close to the fresh gas temperature $T_o$,

$$\frac{T_* - T_o}{T_b - T_o} \ll 1. \tag{5.2}$$

This is equivalent to the assumption that the distance between the vaporization layer at $T_*$ and the reaction layer at $T_b$ is much larger than the characteristic flame thickness, $d$, defined as the distance between $T_e$ and $T_b$, where $T_e$ is defined as $(T_e - T_o)/(T_b - T_o) \equiv 1/e$, see figure 16. In this limit, $\tau_t \ll \tau_*$ and

$$\omega_* \tau_t \ll 1, \tag{5.3}$$

allowing us to limit our study to the low-frequency domain, $\omega\tau_t \ll 1$. However, in order to pick up the cut-off frequency, our low-frequency analysis must include the dominant unsteady effects (5.1), $\omega\tau_* = O(1)$, contrary to the quasi-steady-state approximation used in the first part of Clavin & Sun (1991). In mathematical terms, we use the distinguished limit,

$$\tau_*/\tau_t \to \infty, \quad \omega\tau_t \to 0, \quad \omega\tau_* = O(1). \tag{5.4}$$

We further simplify the analysis with the assumption that the vaporization is confined to a thin sheet at temperature $T_*$. This is the case for the two following conditions:

($a$) the vapour pressure is a strongly increasing function of temperature;

($b$) the liquid and gas phases are in thermodynamic equilibrium.

The first assumption is satisfied for most liquid fuels and the second is fairly accurate when the diffusion time of vapour between neighbouring droplets, $\tau_{diff}$, is much smaller than the transit time, $\tau_{diff} \ll \tau_t$. Figure 16($a$) shows the five zones of the flame structure considered by Clavin & Sun (1991). $Y$ is the mass fraction of fuel vapour in the gas phase. The fuel vapour concentration is negligible in zone (I). The vaporization zone (II), and the chemical reaction zone (IV), are negligibly thin. The subscript $_*$ indicates the value of a variable within the vaporization zone. $T_*$ is the temperature at which the vapour partial pressure of liquid fuel is sufficient to vaporize all the fuel. This temperature is lower than the boiling point of liquid ($\approx 400$ K) if the mass fraction of fuel is sufficiently small. In conclusion, this model is valid for

a fuel-lean mixture of fuel droplets whose radii are of the order of or smaller than 1 μm and for a liquid mass fraction of a few percent $Y_o \approx 5\%$.

This does not correspond exactly to our experimental conditions where $Y_o \leqslant 5\%$ and $r_d \approx 2$ μm. These values were chosen to strengthen the thermo-acoustic instability of spray combustion. The strength of this mechanism is proportional to $\tau_{vis}/\tau_t$ (see (2.16)) with $\tau_{vis}$ increasing as $r_d^2$ (see (A 6)). The particle radius must be large for the mechanism to be strong. As a consequence, the equilibrium condition between gas and liquid phases, $\tau_{diff} \ll \tau_t$, is no longer fully satisfied. This is due to the fact that, for a given mass fraction, the mean distance between droplets increases with the radius. The more general case for droplets of arbitrary size cannot be fully resolved analytically and requires the help of numerical analysis, see for example Buckmaster & Clavin (1992) and also Buckmaster (1993).

In order to fully investigate analytically the effect of this non-equilibrium, we introduce a second model. The vaporization is still confined in a thin zone at the vaporization temperature $T_*$, but the fuel vapour may now coexist with the liquid droplets and freely diffuse into zone (I) where both the vaporization and the condensation rates are frozen. The corresponding flame structure is shown in figure 16(*b*). Our experimental conditions lie between the situations represented by these two models. In the low-frequency limit (5.4), the theoretical analysis presented below shows that the cut-off frequency is independent of the details of the flame structure. The same expression is obtained for both models.

The interaction of the acoustic waves with the internal structure of the flame is easily understood from figure 16. The periodic acceleration associated with a plane acoustic wave propagating normal to the flame surface will give rise to a phase lag between the velocity of the droplets and the velocity of the gas. This phase lag creates a periodic modulation of the flux of fuel vaporized in zone (II). This unsteady flux of vaporized fuel is transported by convection and by diffusion through the gaseous zone (III) and is consumed at a later time in zone (IV), producing a modulation of the combustion rate. The relaxation equation for the droplet velocity, $v_d$,

$$u - v_d = \frac{\mathrm{i}\omega\tau_{vis}}{1 + \mathrm{i}\omega\tau_{vis}} u \approx \mathrm{i}\omega\tau_{vis} u, \tag{5.5}$$

shows that, at low frequency $\omega\tau_{vis} \ll 1$, the flux of vaporized fuel is in phase quadrature with the acoustic velocity, $u$, and hence out of phase with the acoustic pressure in the (first quarter-wavelength of the) tube. For a lean mixture, the heat release rate in (IV) is proportional to the flux of gaseous fuel entering this zone. Hence, to satisfy the Rayleigh criterion, it is necessary that the flux sees a further phase shift of at least $\pi/2$ during the transit from zone (II) to zone (IV). The residence time of the fuel vapour in (III) is $\tau_*$. If the acoustic frequency is very low, $\omega\tau_* \to 0$, zone (III) is in quasi steady state and there is no phase shift between the fuel vaporized in (II) and consumed in (IV). The fluctuations of pressure and heat release rate are out of phase and there is no thermo-acoustic instability. This is shown by the negative values of the transfer function in the low-frequency region in figures 2(*b*) and 14. For the instability to occur, the frequency must be sufficiently high so that zone (III) is *unsteady*, $\omega\tau_* = O(1)$, and introduces a phase shift of more than $\pi/2$. The time delay between vaporization in zone (II) and combustion in zone (IV) is essential for the Rayleigh criterion to be satisfied.

In our experiments, a small amount of gaseous fuel was added to the initial mixture. This will slightly affect the strength of the thermo-acoustic instability but does not modify the cut-off frequency. This is easily understood from the reasoning above. In

order to simplify the presentation, such details are not included in the theoretical analysis presented below.

### 5.2. *Quantitative analysis*

We assume that the mass fraction of droplets is sufficiently small that they do not affect the thermophysical properties of the mixture. This is the case in our experiments, where the liquid mass fraction is typically 3–4%. In order to simplify the presentation, we neglect the effect of the latent heat of vaporization and the effect of a difference between mass and heat diffusivities, which are proven to have only a weak effect on the value of the cut-off frequency. However we will take account of the temperature dependence of the diffusivity, neglected by Clavin & Sun (1991). The details of the corresponding calculations are given in Appendix C. The quantitative solution to the problem is obtained by solving the unsteady energy and mass conservation equations for the fuel, (C 1) and (C 2). The first step in the analysis is to express the instantaneous distribution of the enthalpy of the gaseous phase, $h = C_p T + QY$, where $Q$ is the heat of reaction of the fuel, in terms of the variation of the flame speed. The linear equation, for unity Lewis number, is obtained by summing (C 1) and (C 2). It is to be solved in zones (III), (IV) and (V). Using the mass-weighted space coordinate, $\chi$ (see (C 3)), and the notation of (C 6) in which the bar represents the stationary part of a variable and the hat represents the fluctuating part, this equation takes the form

$$\mathrm{i}\omega\hat{h} + \bar{u}_b \frac{\mathrm{d}}{\mathrm{d}\chi}\hat{h} - \frac{\mathrm{d}}{\mathrm{d}\chi}\left(\bar{\mathscr{D}}\frac{\mathrm{d}}{\mathrm{d}\chi}\hat{h}\right) = 0, \tag{5.6}$$

where $\mathscr{D}$ is a mass-weighted diffusivity, defined in (C 5), and we have used the property of the steady-state solution, $\mathrm{d}\bar{h}/\mathrm{d}\chi = 0$. A general analysis is given in Appendix C. We will limit the presentation in the text to the simpler case where the temperature dependence of the mass-weighted diffusion coefficient, $\mathscr{D}$, is neglected. In the low-frequency limit, the solution of (5.6) which satisfies the downstream condition of non-divergence in the burnt gas, $\chi \to +\infty$, yields an unsteady enthalpy profile which can be expressed in terms of the unknown fluctuation in flame speed, $\hat{\mathscr{U}}_b$, as

$$\chi > \chi_* : \quad \hat{h}(\chi) = 2C_p \frac{(T_b - T_o)}{\beta} \frac{\hat{\mathscr{U}}_b}{\bar{u}_b} \exp\left(-\mathrm{i}\frac{\omega}{\bar{u}_b}\chi\right), \tag{5.7}$$

with $\mathscr{U}_b(t) \equiv u_b - \mathrm{d}\alpha/\mathrm{d}t$, where $u_b$ is the velocity of the gas crossing the reaction zone (gas velocity in burnt gas), $\alpha$ is the coordinate of the reaction sheet (zone (IV)) and $\beta$ is the reduced activation energy, see (2.12), Equation (5.7) is valid downstream from the vaporization zone (II) when $\beta \gg 1$, $\omega\tau_t \ll 1$ and $\omega\chi_*/\bar{u}_b = O(1)$. A more general solution including the effects of the temperature dependence of the diffusion coefficient, $\mathscr{D}$, is given in (C 19).

The second step in the analysis is to use the conservation of enthalpy fluctuations through the vaporization zone (II) at $x = \alpha_*$ (i.e. at $\chi = \chi_*$) to express the fluctuations of the flame speed in terms of the fluctuations of the gas velocity at the vaporization zone. For negligible latent heat, the temperature and its gradient are continuous through the vaporization zone and enthalpy conservation here reduces to the conservation of the mass flux of fuel. Moreover, in the limiting case (5.1), the diffusive fluxes are negligible and fuel mass conservation through zone (II) reduces to the balance of the convective flux of fuel vapour with the mass flux of liquid into zone (II), resulting from the difference of liquid and gas velocities, $\hat{v}_d - \hat{u}_*$,

$$Y_o \rho_* (\hat{v}_d - \hat{u}_*) = \rho_b \bar{u}_b \hat{Y}_{*+}, \tag{5.8}$$

where $Y_o$ is the liquid mass fraction and $\hat{Y}_{*+}$ is the fluctuation of the mass fraction of fuel vapour at the downstream side of the thin vaporization layer (II). In the low-frequency approximation (5.4) in which zone (I) is in a quasi-steady state, equation (5.8) is valid for the two models presented in § 5.1, see figure 16. The detailed calculations are given in Appendix C. In the limit (5.2) the fluctuations of temperature are negligible in zone (II) and so, to leading order, $\hat{h}_{*+} = C_p \hat{T}_{*+} + Q\hat{Y}_{*+} \approx Q\hat{Y}_{*+}$ and $\hat{Y}_{*+}$ is given by (5.7). Equation (5.8) thus yields

$$\rho_* (\hat{v}_d - \hat{u}_*) = \frac{2}{\beta} \rho_b \hat{\mathscr{U}}_b \exp\left(-\mathrm{i}\frac{\omega}{\bar{u}_b}\bar{\chi}_*\right). \tag{5.9}$$

The fluctuation of flame speed is obtained as a linear function of $\hat{u}_*$, the gas velocity fluctuation at zone (II), by using the relaxation equation (5.5), yielding, for $\omega\tau_{vis} \ll 1$,

$$\hat{\mathscr{U}}_b = -\mathrm{i}\omega\tau_{vis}\frac{\rho_*}{\rho_b}\frac{\beta}{2}\hat{u}_* \exp\left(\mathrm{i}\frac{\omega}{\bar{u}_b}\bar{\chi}_*\right). \tag{5.10}$$

The leading order of the unknown transfer function, defined by $Tr \equiv (\hat{u}_b - \hat{u}_*)/\hat{u}_*$ (see § 2.2) is then obtained from (5.10) by noticing that, according to the definition $\hat{\mathscr{U}}_b \equiv (\hat{u}_b - \mathrm{d}\hat{\alpha}/\mathrm{d}t)$ and the equation of evolution $\mathrm{d}\hat{\alpha}/\mathrm{d}t = \hat{u}_*$, one finds $\hat{\mathscr{U}}_b = (\hat{u}_b - \hat{u}_*)$, so that

$$Tr = -(\mathrm{i}\omega\tau_{vis})\left(\frac{\beta}{2}\frac{\rho_*}{\rho_b}\right)\exp\left(\mathrm{i}\frac{\omega}{\bar{u}_b}\bar{\chi}_*\right). \tag{5.11}$$

According to (5.11), the validity of the asymptotic analysis in the limit $\beta \to \infty$ is ensured in the parameter range corresponding to

$$(\omega\tau_{vis})\left(\frac{\beta}{2}\frac{\rho_*}{\rho_b}\right) = O(1), \tag{5.12}$$

from which condition (C 18) follows. Condition (5.12) is verified well in our experiments: $\tau_{vis} \sim 3.10^{-5}$ s, $\omega \sim 5.10^2\,\mathrm{s}^{-1}$, $\rho_*/\rho_b \sim 6$, $\beta \sim 15$, yielding 0.67 for the numerical value in (5.12).

According to (2.19), the instability can develop in the upper part of the tube, where $G > 0$, only if $\mathrm{Im}(Tr) > 0$. Applying this condition to (5.11), it is seen that the cut-off frequency, $\omega_*$, is given by

$$\omega_*\tau_* = \frac{\pi}{2} \quad \text{with} \quad \tau_* = \frac{|\bar{\chi}_*|}{\bar{u}_b}. \tag{5.13}$$

In dimensional coordinates (see (C 3)) we find

$$\frac{\omega_*}{\rho_b\bar{u}_b}\int_{\alpha_*}^{\alpha}\bar{\rho}(x)\mathrm{d}x = \omega_*\int_{\alpha_*}^{\alpha}\frac{\mathrm{d}x}{\bar{u}(x)} = \frac{\pi}{2}, \tag{5.14}$$

which can also be written, introducing the transit time, $\tau_t \equiv d/U_L = D_{th}(T_o)/U_L^2$, as

$$(\omega_*\tau_t)\frac{1}{d}\int_{\alpha_*}^{\alpha}\frac{U_L}{\bar{u}(x)}\mathrm{d}x = \frac{\pi}{2}. \tag{5.15}$$

This result, (5.13)–(5.15), highlights two points.

(*a*) If the distance separating the combustion zone, $x = \alpha$, from the vaporization zone, $x = \alpha_*$, is sufficiently large, $|\alpha - \alpha_*| \gg d$, the cut-off frequency lies effectively in the low-frequency range, $\omega_*\tau_t \ll 1$, as was anticipated at the beginning of our analysis.

(*b*) In this frequency range, the phase lag is essentially due to the convective flux. The unsteady effects of molecular and heat diffusion on the value of the cut-off frequency are negligible. This cut-off frequency is then controlled only by the transit time of gas particles from the vaporization zone to the combustion zone, $\int_{\alpha_*}^{\alpha}[\bar{u}(x)]^{-1}\mathrm{d}x$, which is much larger than the characteristic transit time associated with the steady-state temperature profile,

$$\int_{\alpha_*}^{\alpha}\frac{\mathrm{d}x}{\bar{u}(x)} \gg \frac{D_{th}(T_b)}{\bar{u}_b^2}, \tag{5.16}$$

Noticing that, when $\mathscr{D} = \text{Const.}$, $\bar{u}_b^2/D_{th}(T_b) = U_L^2/D_{th}(T_o)$, the cut-off frequency takes the simpler form

$$\omega_*\tau_t = \frac{\pi/2}{\ln\left((T_b - T_o)/(T_* - T_o)\right)} \tag{5.17}$$

with $\tau_t \equiv D_{th}(T_o)/U_L^2$.

To summarize, equation (5.17) is valid for both flame models (see figure 16) when the vaporization temperature, $T_*$, is sufficiently close to the unburnt gas temperature, $T_* \to T_o$. In this limit, the leading order of the reduced cut-off frequency, $\omega_*\tau_t$, is found to be independent of the details of the flame structure and, due to the logarithm in equation (5.17), its value depends only weakly on the temperatures $T_*$, $T_o$ and $T_b$. It is shown in Appendix C that (5.17) is independent of the value of the latent heat and is also valid for arbitrary temperature dependence of the thermal diffusivity, $D_{th}$.

For our experimental conditions, $T_o = 295\,\mathrm{K}$, $1865 < T_b < 2260\,\mathrm{K}$, $316 < T_* < 328\,\mathrm{K}$, equation (5.17) gives $0.36 < \omega_*\tau_t < 0.38$, reasonably close to our experimental result $\omega_*\tau_t = 0.3$, see figures 14 and 15. This value of the cut-off frequency is small, but not negligibly small, as required by the assumptions leading to (5.17). It would be possible to carry out a perturbation analysis to calculate higher-order corrections to (5.17). However this would not be very useful since, contrary to the leading-order term, the corrective terms depend strongly on the details of the flame structure.

## 6. Conclusions

The comparison of theoretical analyses with the experimental results presented here, concerning the linear growth rate, shows that the primary acoustic instability of flames propagating in tubes is due to a velocity coupling, but of a very different nature in gaseous and spray combustion. In gaseous combustion the velocity coupling involves modifications to the geometry of the flame front, whereas in spray combustion the coupling involves modifications to the internal structure of the flame front.

For premixed spray combustion, the mechanism of velocity coupling to the geometry of the flame front can also produce a primary instability, but experimentally it is seen that, for a droplet radius of a few microns, the spray mechanism is an order of magnitude stronger than the gaseous mechanism and the latter is totally dominated by the former. At a later stage in flame propagation, a secondary instability is observed in both the gaseous and spray cases. This secondary instability is probably driven by the gaseous parametric mechanism described by Searby & Rochwerger (1991), but has not been investigated here.

This thermo-acoustic instability of the spray is an interesting physical example of an instability resulting from the coupling of two structures characterized by very different length scales: several metres for the acoustic wavelength and $\approx 10^{-4}\,\mathrm{m}$ for the flame thickness. However, due to the small Mach number of the flame propagation

speed, the characteristic time scales are similar: $\approx 10^{-3}$ s for the acoustic time and $\approx 10^{-4}$ s for the characteristic time to cross the flame structure, yielding $\omega_a \tau_t \sim 10^{-1}$. For the Rayleigh criterion (phase relationship) to be satisfied, it has been shown that the existence of a relaxation mechanism is necessary for the development of the instability in a spray. The signature of this inner relaxation process has been shown through our experimental results by the existence of a cut-off frequency for the instability, corresponding to a lower bound on the reduced frequency $\omega\tau_t$. The corresponding critical value was found experimentally to be $\omega\tau_t \approx 0.3$ for our spray flames of decane droplets in air. A simple theoretical analysis of this phenomenon has been given. It shows that the critical value, given by (5.17), is universal and depends only weakly on the nature and equivalence ratio of the fuel through a logarithmic function of the vaporization and burnt gas temperatures.

This work was carried out with financial support from the Société Européene de Propulsion and the Centre National d'Etude Spatiales, contract number 92.0075G, and from the French DRET, contract number 92/0074. The authors wish to thank J. Minelli and F. Abetino for their technical assistance.

## Appendix A. Acoustic losses

Acoustic losses depend on the geometry of the combustion chamber, on the nature of the gaseous medium, on the presence of droplets and also on the location of the interface between cold and hot gases. The combustion chamber is cylindrical (diameter $\varnothing$ and length $L$), closed at one end and open at the other. The geometry being fixed, we first consider the homogeneous case with no interface. We study both experimentally and theoretically the acoustic losses with and without droplets. The results are then extended theoretically to the case with an interface.

The acoustic energy per unit volume, $\varepsilon_v$, is related to the fluctuations of velocity, $\delta u$, and pressure, $\delta p$, through the relation (Landau & Lifshitz 1986)

$$\varepsilon_v = \tfrac{1}{2}\rho\delta u^2 + \tfrac{1}{2}\delta p^2/(\gamma p). \tag{A 1}$$

The first term in (A 1) represents the kinetic energy of the fluctuations and the second term their internal energy. Averaged over an acoustic cycle, the contribution of these two terms is the same and it follows that the averaged acoustic energy of the combustion chamber is

$$\bar{\varepsilon} = \iiint \rho\overline{\delta u^2}\,\mathrm{d}^3 r \tag{A 2}$$

In the case without droplets, this energy is mainly dissipated, at the open end of the tube through *radiative losses*, and at the wall through *diffusive losses.*

Radiative losses: At the open end, the fluctuations of velocity are maximum and the tube behaves as a source of gas of strength $S(\delta u)_o$, where $S = \pi\varnothing^2/4$ and $(\delta u)_o$ represents the velocity fluctuations at the open end. It follows that the total intensity of the sound emitted is (Landau & Lifshitz 1986)

$$\overline{\dot{\varepsilon}_{rad}} = \frac{\rho S^2 \overline{(\dot{\delta u})^2}}{4\pi c}. \tag{A 3}$$

From (A 2) and (A 3) the characteristic time of radiative damping, $1/\tau_{rad} \equiv \overline{\dot{\varepsilon}_{rad}}/\bar{\varepsilon}$, can

be expressed as

$$\frac{1}{\tau_{rad}} = \frac{1}{8}\frac{(\omega\varnothing)^2}{cL}. \tag{A 4}$$

The radiative losses are proportional to $\omega^2$ and thus are nine times higher for the first harmonic than for the fundamental mode.

Wall losses: These losses originate in the presence of thermal and viscous boundary layers at the wall. Considering only the lateral walls, the damping rate related to these diffusive processes is

$$\frac{1}{\tau_{wall}} = \sqrt{8}\,\frac{(\omega D_{th})^{1/2}}{\varnothing}[(\gamma - 1) + Pr^{1/2}], \tag{A 5}$$

where $D_{th}$ is the thermal diffusivity and $Pr$ the Prandtl number. The first term in the brackets of (A 5) is related to the thermal boundary layer and the second one to the viscous layer. For diffusive losses, the damping rate is proportional to $\omega^{1/2}$. The large aspect ratio of our combustion chamber allows us to neglect the diffusive losses at the closed end.

Diffusive losses which are associated with the presence of droplets: When the acoustic wave propagates in a spray, new gradients arise around the droplets and introduce three new damping mechanisms associated with the diffusion of momentum, thermal energy and mass. These mechanisms are associated with three characteristic times, $\tau_{vis}$, $\tau_{ther}$ and $\tau_{mass}$, respectively:

$$\tau_{vis} = \frac{2}{9}\frac{\rho_d}{\rho_{gas}}\frac{r_d^2}{\nu}, \quad \tau_{ther} = \frac{1}{3}\frac{\rho_d}{\rho_{gas}}\frac{r_d^2}{D_{th}}, \quad \tau_{mass} = \frac{1}{3}\frac{\rho_d}{\rho_{gas}}\frac{r_d^2}{D_m}. \tag{A 6}$$

In these expressions, $\rho_d$ is the density of the droplets and $r_d$ is their radius; $\nu$, $D_{th}$ and $D_m$ represent the kinematic viscosity of the gas, the thermal diffusive coefficient in the gas and the mass diffusive coefficient of the vapour in the gas respectively. Following Marble & Candel (1975), the reduced damping rate, $1/(\omega\tau_{drop})$, due to the droplets can then be expressed as the sum of three Lorentzian functions centred on the characteristic times presented above:

$$\frac{1}{\tau_{drop}} \approx \omega\left[x_l\frac{\omega\tau_{vis}}{1+(\omega\tau_{vis})^2} + c_1 x_l\frac{d_1\omega\tau_{ther}}{1+(d_1\omega\tau_{ther})^2} + c_2 x_v\frac{d_2\omega\tau_{mass}}{1+(d_2\omega\tau_{mass})^2}\right]. \tag{A 7}$$

In this expression, $x_l$ is the liquid mass fraction, $x_v$ the vapour mass fraction, and $c_1$, $d_1$, $c_2$ and $d_2$ are four characteristic constants which are lengthy functions of the thermodynamic properties of the two phases and are given in Marble & Candel (1975). In our experiments the numerical evaluations give typically $c_1 \approx 0.9$, $d_1 \approx 2$, $c_2 \approx 3 \times 10^{-3}$ and $d_2 \approx 15$.

The total acoustic loss, $1/\tau_{loss}$, associated with these different mechanisms is given by:

$$\frac{1}{\tau_{loss}} \equiv \frac{1}{\tau_{rad}} + \frac{1}{\tau_{wall}} + \frac{1}{\tau_{drop}}. \tag{A 8}$$

This characteristic damping time can be measured experimentally, using a pulse generator and a loudspeaker placed outside the tube at the open end (typically one diameter outside) and a pressure sensor placed at the closed end. Typically, the energy spectrum obtained presents several peaks corresponding to the different harmonics

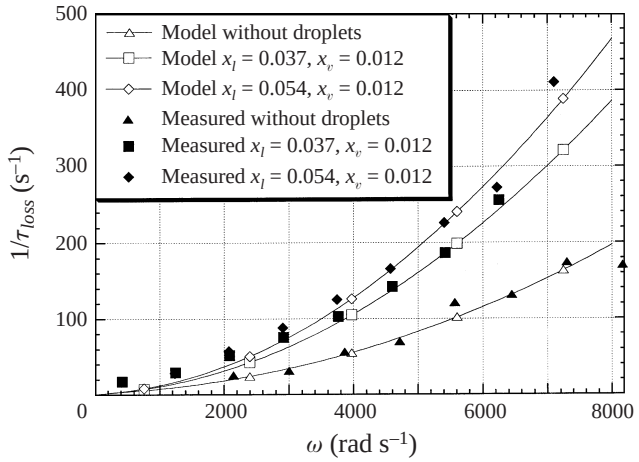


FIGURE 17. Comparison between the acoustic losses measured and calculated from the model, $x_l$ and $x_v$ are the liquid and fuel vapour mass fractions respectively.

of the tube. The shape of each peak follows the law

$$|\delta\hat{p}_n(\omega)|^2 = \frac{4\tau_{loss,n}^2 \delta p_n^2}{1 + 4\tau_{loss,n}^2(\omega_n - \omega)^2}, \tag{A 9}$$

where $n$ is the harmonic number, $\omega_n$ its frequency, $\delta p_n$ its amplitude and $\tau_{loss,n}$, the characteristic damping time at this frequency. Equation (A 9) has been used to measure the damping rate at each harmonic frequency $\omega_n$. Figure 17 presents the comparison between the measured values of the damping rate and the values expected from the analysis presented above for the cases with and without droplets. Except for the fundamental mode, all values agree within 10%. The reason for the relative discrepancy observed on the fundamental mode is not clear.

When the flame front propagates in the combustion chamber, it is not possible to measure the acoustic losses experimentally since the system is not passive but has internal gain. Consequently, we have evaluated the characteristic frequencies and the total acoustic losses, as a function of the flame position, using a two-zone calculation for a passive system (Clanet 1995). The calculated losses were then renormalized by the ratio of measured to calculated losses without the flame. This heuristic correction was small except for the fundamental frequency. In figure 18($a$) and 18($b$) we show the acoustic losses for the two cases, without and with droplets, calculated as a function of the relative position of the interface, $r$. The losses are normalized by the acoustic time, $\tau_a \equiv L/c_0$. In the spray case, the losses are calculated for a liquid mass fraction $x_l = 0.054$ and a vapour mass fraction $x_v = 0.012$. When the front reaches the closed end of the tube ($r \approx 0$), there is no difference between the cases with and without droplets.

## Appendix B. Coupling between acceleration field and cellular flames

Pelcé & Rochwerger (1992) have calculated the growth rate of an acoustic instability driven by the effect of the acoustic acceleration on the geometry of the flame front. In this mechanism, the amplitude of cellular structures is modulated by the periodic acoustic acceleration of the gas. This leads to a corresponding modulation of the

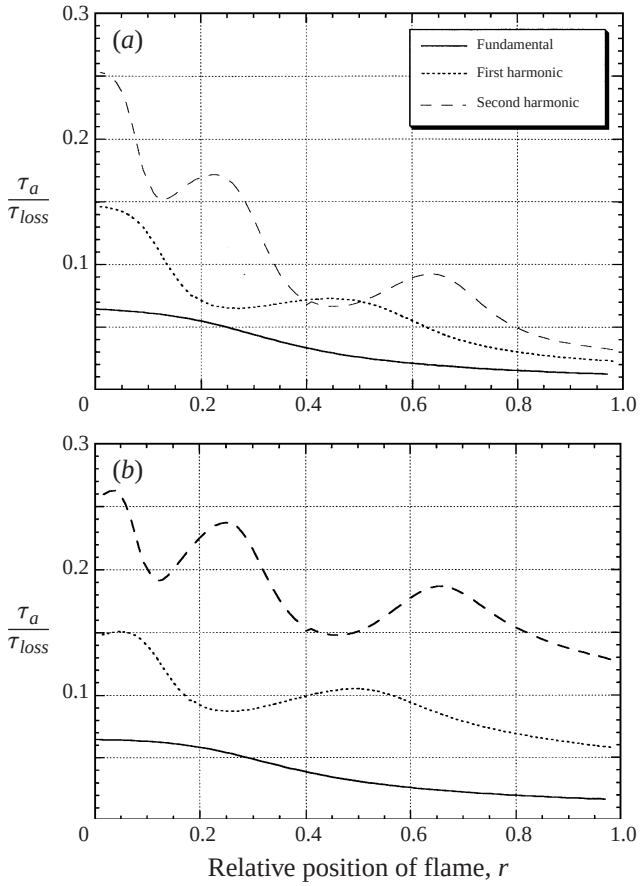


FIGURE 18. Acoustic losses without droplets (*a*) and with droplets (*b*), as a function of the relative position of the interface. Calculated for an equivalence ratio 1.0 ($x_l = 0.054$).

total flame surface area and thus to a modulation of the global heat release rate. In order to simplify their analysis, they have used a laminar flame model in which all diffusion coefficients are assumed to be temperature independent. They have treated the case of a flame front which is planar on average, but perturbed by a two-dimensional sinusoidal wrinkling of small amplitude. Such flames have been observed at the threshold of planar stability for downwards propagating flames (Searby & Quinard 1990). Pelcé & Rochwerger have assumed that the flame is wrinkled at the marginally unstable wavenumber. They give the following expression for the relative instantaneous perturbation to the amplitude of wrinkling (their equation (19)):

$$Q = \frac{-\mathrm{i}\omega\tau_t\, C(kd)}{-(\omega\tau_t)^2\, A(kd) + \mathrm{i}\omega\tau_t\, B(kd) + D(kd)}\, a\frac{u}{U_L}, \tag{B 1}$$

where $\omega\tau_t$ and $kd$ are the reduced acoustic frequency and reduced wavenumber of wrinkling respectively, $a$ is the amplitude of wrinkling, $u$ is the acoustic velocity and $U_L$ the laminar flame speed. The functions $A(kd)$, $B(kd)$, $C(kd)$ and $D(kd)$ are terms in the dispersion relation for the laminar flame, given explicitly in their paper. The dispersion relation for the corresponding flame model with temperature-dependent diffusivities has been given by Clavin & Garcia (1983). The same dispersion relation,

in the present notation, can also be found in Searby & Clavin (1986). For the case of temperature-dependent diffusivities, the functions $A(kd)$–$D(kd)$ are given by

$$A(kd) = (2-\gamma) + \gamma\, kd\left(Ma - \mathscr{J}/\gamma\right), \tag{B 2}$$

$$B(kd) = 2kd + \frac{2(kd)^2}{(1-\gamma)}\left(Ma - \mathscr{J}\right), \tag{B 3}$$

$$C(kd) = \gamma\, kd\left[1 - kd\left(Ma - \mathscr{J}/\gamma\right)\right] \tag{B 4}$$

$$D(kd) = \frac{\gamma\, kd}{Fr}\left[1 - kd\left(Ma - \mathscr{J}/\gamma\right)\right] - \frac{\gamma}{(1-\gamma)} \times \left[(kd)^2 + (kd)^3\left(h_b + \frac{(2+\gamma)}{\gamma}Ma - 2\mathscr{J}/\gamma + (2Pr-1)\int_0^1 (h_b - h(\theta)\mathrm{d}\theta\right)\right]. \tag{B 5}$$

In these expressions, $Ma$, $Fr$ and $Pr$ are the Markstein, Prandtl and Froude numbers respectively, $\gamma$ is the reduced gas expansion ratio, $\theta$ is the reduced temperature, $h(\theta)$ is the density-weighted thermal diffusivity normalized by its value in the unburnt gas, $h_b$ is the reduced density-weighted thermal diffusivity in the burnt gas and $\mathscr{J} = \gamma/(1-\gamma)\int_0^1 h(\theta)/(1+\theta\gamma/(1-\gamma))\mathrm{d}\theta$. The reader is referred to the cited literature for further details. At the threshold of stability of the planar flame, the marginally unstable wavenumber, $k_c$, is given by $D(k_c d) = 0$.

In order to compare our experimental results with the growth rate calculated for this mechanism, we have extended the work of Pelcé & Rochwerger in two ways. First, we have used the above expressions for $A(kd)$–$D(kd)$ in place of the expressions in their paper, based on temperature-independent diffusivities. Second, we have relaxed their assumption that the cell size is given by the marginally unstable wavenumber, $D(k_c d) = 0$. This leads to the following expression for the transfer function, our equation (2.15):

$$Tr = \frac{(ak)^2}{2}\left(\frac{T_b - T_o}{T_o}\right)\frac{-\mathrm{i}\omega\tau_t\, C(kd)}{-(\omega\tau_t)^2\, A(kd) + \mathrm{i}\omega\tau_t\, B(kd) + D(kd)}. \tag{B 6}$$

Equation (B 6) should be realistic for real flames with a high activation energy and small-amplitude sinusoidal wrinkling, $ka \ll 1$, at arbitrary wavenumber.

In our experiments the flame wrinkling was not sinusoidal, but cusped, see figure 19. This is not a fundamental limitation since any shape of flame front may be represented, by Fourier decomposition, as a superposition of sinusoidal wrinkles. The global growth rate of the instability can be found by summing the sum of the growth rates for each wavenumber of the decomposition. However the aspect ratio of the wrinkling in the experiments was also not small, typically $ak \approx 0.5$, outside the strict domain of validity of the calculation. Nevertheless, we have used the measured values of the average cell size (often equal to the tube diameter, 0.1 m) and the measured cell amplitude in equation (B 6). In view of the fact that the cell aspect ratio was not small, we did not consider it useful to treat the flame shape by Fourier decomposition, mentioned above. The calculated value is thus only an estimation of the growth rate for this mechanism. However we still expect this calculation to give the correct order of magnitude.

In § 4 we have used a Markstein number equal to 4. This is the value that has been measured experimentally for lean propane flames (Clanet & Searby 1998; Searby & Rochwerger 1991). The flame temperature, the gas expansion ratio, terms involving the temperature dependence of transport coefficients and other thermodynamic gas

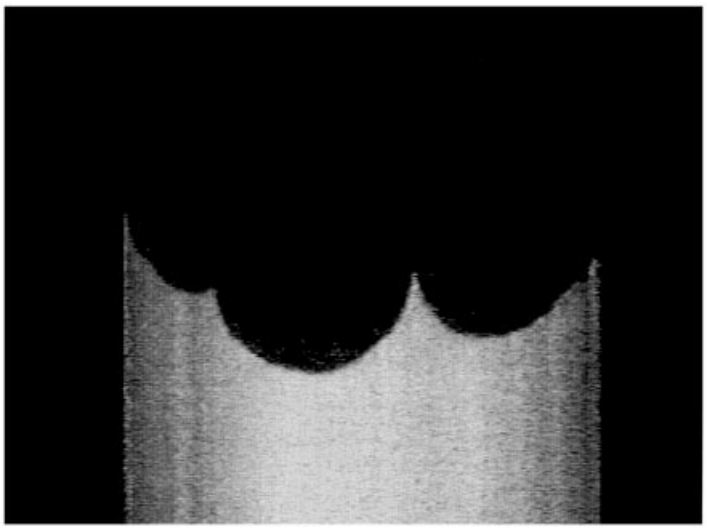

FIGURE 19. Tomographic cut through cellular propane-air flame at onset of acoustic instability. Equivalence ratio = 0.8, $U_L = 0.3\ \mathrm{m\,s^{-1}}$.

data were calculated for each mixture composition using the CHEMKIN package and its thermodynamic database. No arbitrary or adjustable values were used for any of the parameters in the calculation. A typical set of parameters calculated for an equivalence ratio of 0.85 was: $U_L = 0.34\ \mathrm{m\,s^{-1}}$, $T_b = 2123$ K, $h_b = 3.64$ (ratio of diffusivities in burnt and unburnt gases), $\int_0^1 (h_b - h(\theta)\mathrm{d}\theta = 1.16$, $\mathscr{J} = 4.11$, $D_{th} = 0.21$, $Pr = 0.695$.

## Appendix C. Calculation with temperature-dependent diffusivities

We suppose that the flame is quasi-isobaric and we neglect the effect of the latent heat of vaporization of the liquid fuel. The equation for the conservation of energy, in planar geometry, can be written

$$\rho\frac{\partial T}{\partial t} + \rho u\frac{\partial T}{\partial x} - \frac{\partial}{\partial x}\left[(\rho D)\frac{\partial T}{\partial x}\right] = \rho_b\frac{Q}{C_p}W(T,Y), \tag{C 1}$$

where $W$ is the chemical reaction rate and $Q$ is the heat of reaction per unit mass of fuel. The mass conservation equation for the species limiting the reaction in the gas phase is

$$\rho\frac{\partial Y}{\partial t} + \rho u\frac{\partial Y}{\partial x} - \frac{\partial}{\partial x}\left[(\rho D)\frac{\partial Y}{\partial x}\right] = -\rho_b W(T,Y), \tag{C 2}$$

where we have used the hypothesis of unity Lewis number ($D_{th} = D_m \equiv D$), and $\rho_b$ is the density of the burnt gas corresponding to the steady-state solution. We introduce the mass-weighted axial space coordinate:

$$\chi = \frac{1}{\rho_b}\int_{\alpha(t)}^{x}\rho(x,t)\mathrm{d}x, \quad \frac{\partial}{\partial x} = \left(\frac{\rho}{\rho_b}\right)\frac{\partial}{\partial\chi}, \tag{C 3}$$

where $x = \alpha(t)$ is the position of the thin reaction zone. In the planar unsteady case, when the effect of production of fuel vapour is neglected,

$$\frac{\partial \rho}{\partial t} + \frac{\partial (\rho u)}{\partial x} = 0,$$

this classical transformation simplifies the expressions for the one-dimensional unsteady conservation equations. Mass conservation shows that the following equality is true everywhere in the gas phase:

$$\rho \frac{\partial}{\partial t} + \rho u \frac{\partial}{\partial x} - \frac{\partial}{\partial x}\left[(\rho D)\frac{\partial}{\partial x}\right] \equiv \rho_b \left[\frac{\partial}{\partial t} + \mathscr{U}_b \frac{\partial}{\partial \chi} - \frac{\partial}{\partial \chi}\left(\mathscr{D}(T)\frac{\partial}{\partial \chi}\right)\right], \tag{C 4}$$

where

$$\mathscr{U}_b(t) \equiv u_b - \frac{\mathrm{d}\alpha}{\mathrm{d}t}$$

is the velocity of the gas crossing the reaction zone (gas velocity in burnt gas), and by definition,

$$\mathscr{D}(T) \equiv \left(\frac{\rho}{\rho_b}\right)^2 D(T), \tag{C 5}$$

which will be considered to be a function of temperature, using the perfect gas law in the quasi-isobar approximation.

We now use the linear decomposition

$$a = \bar{a} + \hat{a}, \tag{C 6}$$

where $\bar{a}$ is the value of the steady-state solution and $\hat{a}$ is the unsteady perturbation. Outside the combustion zone, IV, (C 1) then gives

$$\frac{\partial \hat{T}}{\partial t} + \bar{u}_b \frac{\partial \hat{T}}{\partial \chi} - \frac{\partial}{\partial \chi}\left(\bar{\mathscr{D}}\frac{\partial \hat{T}}{\partial \chi}\right) - \frac{\partial}{\partial \chi}\left(\frac{\partial \bar{\mathscr{D}}}{\partial T}\hat{T}\frac{\partial \bar{T}}{\partial \chi}\right) = -\hat{\mathscr{U}}_b(t)\frac{\mathrm{d}\bar{T}}{\mathrm{d}\chi}. \tag{C 7}$$

Using the time Fourier transform, (C 7) becomes

$$\mathrm{i}\omega \hat{T} + \bar{u}_b \frac{\mathrm{d}\hat{T}}{\mathrm{d}\chi} - \frac{\mathrm{d}^2}{\mathrm{d}\chi^2}\left(\bar{\mathscr{D}}\hat{T}\right) = -\hat{\mathscr{U}}_b(\omega)\frac{\mathrm{d}\bar{T}}{\mathrm{d}\chi}. \tag{C 8}$$

The particular solution to (C 8) is

$$-\frac{\hat{\mathscr{U}}_b(\omega)}{\mathrm{i}\omega}\frac{\mathrm{d}\bar{T}}{\mathrm{d}\chi}, \tag{C 9}$$

and the steady-state solution satisfies the equations

$$\bar{U}_b \frac{\mathrm{d}\bar{Y}}{\mathrm{d}\chi} - \frac{\mathrm{d}}{\mathrm{d}\chi}\left(\bar{D}\frac{\mathrm{d}\bar{Y}}{\mathrm{d}\chi}\right) = 0, \quad \bar{U}_b \frac{\mathrm{d}\bar{T}}{\mathrm{d}\chi} - \frac{\mathrm{d}}{\mathrm{d}\chi}\left(\bar{D}\frac{\mathrm{d}\bar{T}}{\mathrm{d}\chi}\right) = 0. \tag{C 10}$$

The solutions in the external zone are

$\chi < 0$ : (in the gaseous zone, (III))

$$\Theta \equiv \left(1 - \frac{\bar{Y}}{Y_o}\right) = \left(\frac{\bar{T} - T_o}{T_b - T_o}\right) = \exp\left(\int_0^{\chi'} \frac{\bar{u}_b}{\bar{\mathscr{D}}}\mathrm{d}\chi'\right) = \exp(\xi) \tag{C 11}$$

$\chi > 0$ : (in the burnt gas zone, (IV))

$$\bar{Y} = 0, \quad \bar{T} = T_b,$$

where $Y_o$ is the mass fraction of fuel in the unburnt gas, and where we have introduced the non-dimensional mass-weighted space coordinate, $\xi$, defined by

$$\xi \equiv \int_0^{\chi'} \frac{\bar{u}_b}{\bar{\mathscr{D}}} \mathrm{d}\chi', \quad \mathrm{d}\xi = \frac{\bar{u_b}}{\bar{\mathscr{D}}} \mathrm{d}\chi. \tag{C 12}$$

The solution to the enthalpy conservation equation (5.6) is obtained in the low-frequency limit by the WKB method, $\hat{h} = \mathrm{e}^S$, by expansion in the small parameter $\omega \bar{\mathscr{D}}_b / \bar{u}_b^2 \ll 1$, where $\bar{\mathscr{D}}_b \equiv \bar{\mathscr{D}}(T_b)$, and to the leading order we find

$$\mathrm{i} \frac{\omega}{\bar{u}_b^2} \mathscr{D}_b \left( \frac{\bar{\mathscr{D}}}{D_b} \right) + \frac{\mathrm{d}S}{\mathrm{d}\xi} - \frac{\mathrm{d}^2 S}{\mathrm{d}\xi^2} = 0. \tag{C 13}$$

The solution to (C 13) which satisfies the condition of non-divergence for $\chi \to +\infty$ (in the burnt gas) is

$$\hat{h}(\xi) = \hat{h}(0) \exp \left\{ \mathrm{i}\omega \frac{\mathscr{D}_b}{\bar{u}_b^2} \left[ -\xi + \int_\xi^0 \left( \frac{\bar{\mathscr{D}}}{\mathscr{D}_b} - 1 \right) \mathrm{d}\xi' - \mathrm{e}^\xi \int_\xi^0 \mathrm{e}^{-\xi'} \left( \frac{\bar{\mathscr{D}}}{\mathscr{D}_b} - 1 \right) \mathrm{d}\xi' \right] \right\}. \tag{C 14}$$

The solution (C 14) is valid when the temperature is greater than the vaporization temperature, $T > T_*$, i.e. in the zones (III), (IV), and (V) of figure 16. The temperature fluctuation, $\hat{T}(\chi, \omega)$, is given by the solution to the linear equation (C 7), which, at low frequencies, can be written

$\chi < 0$ :

$$\hat{T} = \hat{\mathscr{U}}_b \bar{u}_b \frac{(T_b - T_o)}{\mathscr{D}} \mathrm{e}^\xi \frac{1}{\mathrm{i}\omega} \left[ \exp \left( \frac{\mathrm{i}\omega}{\bar{u}_b} \chi \right) - 1 \right] + \hat{T}(0) \frac{\mathscr{D}_b}{\mathscr{D}} \exp \left( \xi + \frac{\mathrm{i}\omega}{\bar{u}_b} \chi \right), \tag{C 15}$$

$\chi > 0$ :

$$\hat{T} = \hat{T}(0) \exp \left( - \frac{\mathrm{i}\omega}{\bar{u}_b} \chi \right), \tag{C 16}$$

where we have used the particular solution (C 9) and the low-frequency expansion of the solutions to the homogeneous equation, (C 7), which satisfy the boundary conditions at $x \to +\infty$ in (C 16) and at $x \to -\infty$ in (C 15).

In the framework of the theory of Zeldovich & Frank-Kamenetskii (1938), adapted to cover the unsteady case (Joulin & Clavin 1979), the relative fluctuation of the combustion temperature, $\hat{T}(0)$, is assumed to be of the order of the inverse of the reduced activation energy, $\beta$, a condition which can be verified only in a particular range of parameters defined by (5.12). In the limit $\beta \to \infty$, the relation between the fluctuations of heat flux into the preheat zone and the combustion temperature is controlled by the combustion kinetics in zone (IV),

$$\left. \frac{\mathrm{d}}{\mathrm{d}\xi} \hat{T} \right|_{\xi = 0_-} = \frac{\beta}{2} \hat{T}(0). \tag{C 17}$$

The calculation of the heat flux from (C 15) gives the modification to the flame burning velocity, to leading order in the limit $\beta \to \infty$:

$$\frac{\hat{\mathscr{U}}_b}{\bar{\mathscr{U}}_b} = \frac{\beta}{2} \frac{\hat{T}(0)}{T_b - T_o}. \tag{C 18}$$

Choosing the position of the origin in the internal zone (IV) where $\hat{Y} = 0$, $\hat{h}(0) = C_p\hat{T}(0)$, we can rewrite (C 14) in the region where $\xi > \xi_*$ in the form

$$\hat{h} = 2C_p\frac{(T_b - T_o)}{\beta}\frac{\hat{\mathscr{U}}_b}{\bar{u}_b}\exp\left\{\mathrm{i}\omega\frac{\mathscr{D}_b}{\bar{u}_b^2}\left[-\xi + \int_\xi^0\left(\frac{\bar{\mathscr{D}}}{\mathscr{D}_b} - 1\right)\mathrm{d}\xi'\right.\right.$$
$$\left.\left. -\mathrm{e}^{\xi}\int_\xi^0 \mathrm{e}^{-\xi'}\left(\frac{\bar{\mathscr{D}}}{\mathscr{D}_b} - 1\right)\mathrm{d}\xi'\right]\right\}. \quad \text{(C 19)}$$

Equation (C 19) takes the much simpler form (5.7), when the temperature dependence of the mass-weighted diffusivity, $\mathscr{D}$, is neglected.

Assuming that the vaporization takes place at the fixed temperature $T = T_*$, the position of the vaporization zone of figure 16,

$$\chi_*(t) \equiv \frac{1}{\rho_b}\int_{\alpha(t)}^{\alpha_*(t)}\rho(x', t)\,\mathrm{d}x' \quad \text{(C 20)}$$

is given by $T(\chi = \chi_*) = T_*$,

$$\hat{T}(\bar{\chi}_*) + \hat{\chi}_*\left.\frac{\mathrm{d}\bar{T}}{\mathrm{d}\chi}\right|_{\chi=\bar{\chi}_*} = 0, \quad \text{(C 21)}$$

and thus the speed of this front, $\mathrm{d}\hat{\chi}_*/\mathrm{d}t$, in the laboratory frame is

$$\frac{\mathrm{d}\hat{\chi}_*}{\mathrm{d}t} = -\mathrm{i}\omega\left[\hat{T}(\bar{\chi}_*)\Big/\left(\left.\frac{\mathrm{d}\bar{T}}{\mathrm{d}\chi}\right|_{\chi=\bar{\chi}_*}\right)\right]. \quad \text{(C 22)}$$

According to (C 20) and mass conservation, the gaseous mass flux through the vaporization front is

$$\rho_*\left(u_* - \frac{\mathrm{d}\hat{\alpha}_*}{\mathrm{d}t}\right) = \rho_b\left(\mathscr{U}_b - \frac{\mathrm{d}\hat{\chi}_*}{\mathrm{d}t}\right), \quad \text{(C 23)}$$

where $\mathscr{U}_b(t) \equiv u_b - \mathrm{d}\alpha/\mathrm{d}t$. The flux of any quantity $Z$ through the vaporization zone,

$$f_{*+}^{(Z)} = \rho_*\left(u_* - \frac{\mathrm{d}\hat{\alpha}_*}{\mathrm{d}t}\right)Z_* - \rho_* D_*\left.\frac{\partial Z}{\partial x}\right|_{x=\alpha_{*+}}$$

can be written, using (C 23) and (C 3)

$$f_{*+}^{(Z)} = \rho_b\left(\mathscr{U}_b - \frac{\mathrm{d}\hat{\chi}_*}{\mathrm{d}t}\right)Z_* - \rho_b\mathscr{D}_*\left.\frac{\partial Z}{\partial \chi}\right|_{\chi=\chi_{*+}}. \quad \text{(C 24)}$$

The mass flux of liquid fuel into the vaporization zone is

$$m_d n_d\left(v_d - \frac{\mathrm{d}}{\mathrm{d}t}\hat{\alpha}_*(t)\right),$$

where $m_d$, $n_d$ and $v_d$ are the mass, number density and velocity of the droplets respectively. Using (C 23), the mass flux of liquid can be written as a function of the gas velocity in the vaporization zone, $u_*$:

$$m_d n_d\left(v_d - \frac{\mathrm{d}}{\mathrm{d}t}\hat{\alpha}_*(t)\right) = m_d n_d(v_d - u_*) + \frac{\rho_b}{\rho_*}m_d n_d\left(\mathscr{U}_b - \frac{\mathrm{d}}{\mathrm{d}t}\hat{\chi}_*(t)\right). \quad \text{(C 25)}$$

Introducing the diffusive and convective fluxes of fuel vapour leaving the vaporization

zone, the conservation of fuel through the vaporization zone can be written, for the first flame model of figure 16(*a*),

$$Y_o\,\rho_*\,(v_d-u_*)+\rho_b\,(Y_o-Y_{*+})\left(\mathscr{U}_b-\frac{\mathrm{d}\hat{\chi}_*}{\mathrm{d}t}\right)=-\rho_b\mathscr{D}_*\left.\frac{\mathrm{d}Y}{\mathrm{d}\chi}\right|_{\chi=\chi_{*+}},\qquad(\mathrm{C}\,26)$$

in which we have introduced the liquid mass fraction, $Y_o\equiv m_d n_d/\rho_0$. The linearized expansion of (C 26) gives

$$\begin{aligned}Y_o\,\rho_*\,(\hat{v}_d-\hat{u}_*)+\rho_b\,\left(Y_o-\bar{Y}_{*+}\right)\left(\hat{\mathscr{U}}_b-\frac{\mathrm{d}\hat{\chi}_*}{\mathrm{d}t}\right)-\bar{u}_b\,\rho_b\hat{Y}\left|_{\chi=\bar{\chi}_{*+}}\right.\\ =+\rho_b\hat{\chi}_*\left[\bar{\mathscr{U}}_b\left.\frac{\mathrm{d}\bar{Y}}{\mathrm{d}\chi}\right|_{\chi=\bar{\chi}_{*+}}-\mathscr{D}_*\left.\frac{\mathrm{d}^2\bar{Y}}{\mathrm{d}\chi^2}\right|_{\chi=\bar{\chi}_{*+}}\right]-\rho_b\mathscr{D}_*\left.\frac{\mathrm{d}\hat{Y}}{\mathrm{d}\chi}\right|_{\chi=\bar{\chi}_{*+}},\qquad(\mathrm{C}\,27)\end{aligned}$$

where the first term on the right-hand side can be calculated from (C 10) and (C 22) to give

$$\begin{aligned}Y_o\,\rho_*\,(\hat{v}_d-\hat{u}_*)+\rho_b\,\left(Y_o-\bar{Y}_{*+}\right)\left(\hat{\mathscr{U}}_b-\frac{\mathrm{d}\hat{\chi}_*}{\mathrm{d}t}\right)\\ =\bar{u}_b\,\rho_b\hat{Y}\left|_{\chi=\bar{\chi}_{*+}}\right.-\rho_b\mathscr{D}_*\left.\frac{\mathrm{d}\hat{Y}}{\mathrm{d}\chi}\right|_{\chi=\bar{\chi}_{*+}}+\rho_b Y_o\frac{\hat{T}(\bar{\chi}_*)}{(T_b-T_o)}\left.\frac{\mathrm{d}\mathscr{D}}{\mathrm{d}\chi}\right|_{\chi=\bar{\chi}_{*+}},\qquad(\mathrm{C}\,28)\end{aligned}$$

where $\hat{T}(\chi_*)$ is given by (C 15), $\hat{Y}_{*+}\equiv\hat{Y}\left|_{\chi=\chi_{*+}}\right.$ and $\mathrm{d}\hat{Y}/\mathrm{d}\chi\left|_{\chi=\bar{\chi}_{*+}}\right.$ are obtained from (C 19) using $\hat{h}=Q\hat{Y}+C_p\hat{T}$, and $\mathrm{d}\hat{\chi}_*/\mathrm{d}t$ is given by (C 22). The transfer function is then obtained from (C 28) when the relaxation relation (5.5) is used.

The problem simplifies greatly in the distinguished limit $\omega\tau_t\to 0$, $\xi_*\to-\infty$, $(\omega\tau_t)\xi_*=O(1)$, which is relevant when $T_*\to T_o$. In this limit, the exponent on the right-hand side of (C 19) reduces to

$$\mathrm{i}\omega\frac{\mathscr{D}(T_o)}{\bar{u}_b^2}\xi_*=\mathrm{i}\omega\frac{\rho_o^2 D(T_o)}{\rho_b^2\bar{u}_b^2}\xi_*=\mathrm{i}\omega\tau_t\xi_*,$$

the latter equality resulting from $\rho_b\bar{u}_b=\rho_o U_L$. Moreover, according to (C 11) and (C 15), $\hat{T}_*(\chi_*)$ and $\left(Y_o-\bar{Y}_{*+}\right)$ are proportional to the transcendentally small term $\exp(\xi_*)$ and are thus negligible. Notice also that, for the same reason, a non-zero latent heat of vaporization has no effect in this limit. Finally notice that $\mathscr{D}_*\mathrm{d}\hat{Y}/\mathrm{d}\chi|_{\chi_{*+}}$ is negligible compared to $\hat{Y}(\chi_{*+})$ so that we find exactly the same results as (5.11) and (5.17).

In the second flame model of figure 16(*b*), the conservation of fuel through the vaporization zone yields

$$m_d n_d\left(v_d-\frac{\mathrm{d}}{\mathrm{d}t}\hat{\alpha}_*(t)\right)=\rho_b D_*\left[\left.\frac{\mathrm{d}Y}{\mathrm{d}\chi}\right|_{\chi=\chi_{*-}}-\left.\frac{\mathrm{d}Y}{\mathrm{d}\chi}\right|_{\chi=\chi_{*+}}\right],\qquad(\mathrm{C}\,29)$$

which, in the low-frequency limit (5.4), reduces to the same equation as for the first flame model:

$$m_d n_d\left(v_{\mathrm{d}}-\frac{\mathrm{d}}{\mathrm{d}t}\hat{\alpha}_*(t)\right)=\rho_b\left(v_b-\frac{\mathrm{d}\hat{\chi}_*}{\mathrm{d}t}\right)Y_*-\rho_b D_*\left.\frac{\mathrm{d}Y}{\mathrm{d}\chi}\right|_{\chi=\chi_{*+}}\qquad(\mathrm{C}\,30)$$

because zone (I) is quasi steady in this limit. The final results are thus the same for both models.

## REFERENCES


Bayvel, L. & Jones, A. 1981 *Electromagnetic Scattering and its Applications*. London: Applied Science Publishers.

Buckmaster, J. 1993 The structure and stability of laminar flames. *Ann. Rev. Fluid Mech.* **25**, 21–53.

Buckmaster, J. & Clavin, P. 1992 An acoustic instability theory for particle-cloud flames. In *Twenty-fourth Symp. (Intl) on Combustion, Sydney, Australia*, pp. 29–36. The Combustion Institute, Pittsburgh.

Clanet, C. 1995 Instabilités de propagation de flammes monophasiques et diphasiques dans une enceinte semi-ouverte. PhD thesis, Université d'Aix-Marseille-I.

Clanet, C. & Searby, G. 1998 First experimental study of the darrieus-landau instability. *Phys. Rev. Lett.* **27**, 3867–3870.

Clavin, P. 1994 Premixed combustion and gasdynamics. *Ann. Rev. Fluid Mech.* **26**, 321–352.

Clavin, P. & Garcia, P. 1983 The influence of the temperature dependence of diffusivities on the dynamics of flame fronts. *J. Méc. Théor. Appl.* **2**, 245–263.

Clavin, P., Pelcé, P. & He, L. 1990 One-dimensional vibratory instability of planar flames propagating in tubes. *J. Fluid Mech.* **216**, 299–322.

Clavin, P. & Siggia, E. D. 1991 Turbulent premixed flames and sound generation. *Combust. Sci. Technol.* **78**, 147–155.

Clavin, P. & Sun, J. 1991 Theory of acoustic instabilities of planar flames propagating in sprays or particle-laden gases. *Combust. Sci. Technol.* **78**, 265–288.

Dunlap, R. 1950 Resonance of flames in a parallel-walled combustion chamber. *Tech. Rep.* Project MX833, Report UMM-43. Aeronautical Research Center. University of Michigan.

Joulin, G. & Clavin, P. 1979 Linear stability analysis of nonadiabatic flames: diffusional-thermal model. *Combust. Flame* **35**, 139–153.

Kaskan, W. 1953 An investigation of vibrating flames. In *Fourth Intl Symp. on Combustion*, pp. 575–591. Williams and Wilkins, Baltimore.

Kee, R., Miller, J. & Jefferson, T. 1980 Chemkin: A general-purpose, problem-independent, transportable, fortran chemical kinetics code package. *Rep.* SAND80-8003. Sandia National Laboratories.

Kee, R., Rupley, F. & Miller, J. 1990 The chemkin thermodynamic data base. *Rep.* SAND87-8215B. Sandia National Laboratories.

Landau, L. & Lifshitz, E. 1986 *Fluid Mechanics*, 1st edn. Pergamon.

Law, C. 1982 Recent advances in droplet vaporization and combustion. *Prog. Energy Combust. Sci.* **8**, 171–201.

Leyer, J.-C. & Manson, N. 1971 Development of vibratory flame propagation in short closed tubes and vessels. In *Thirteenth Symp. (Intl) on Combustion*, pp. 551–557. The Combustion Institute, Pittsburgh.

Mallard, E. & Le Chatelier, H. 1883 Recherches expérimentales et théoriques sur la combustion des mélanges gazeux explosifs. *Ann. Mines, Paris* **8** (4), 274–377.

Marble, F. & Candel, S. 1975 Acoustic attenuation in fans and ducts by vaporization of liquid droplets. *AIAA J.* **13**, 634–639.

Markstein, G. 1953 Instability phenomena in combustion waves. In *Fourth Intl Symp. on Combustion*, pp. 44–59. Williams and Wilkins, Baltimore.

Markstein, G. 1964 *Nonsteady Flame Propagation*. Pergamon.

Markstein, G. 1970 Flames as amplifiers of fluid mechanical disturbances. In *Proc. Sixth Natl Congr. Appl. Mech.*, pp. 11–33. Cambridge, Mass.

Pelcé, P. & Clavin, P. 1982 Influence of hydrodynamics and diffusion upon the stability limits of laminar premixed flames. *J. Fluid Mech.* **124**, 219–237.

Pelcé, P. & Rochwerger, D. 1992 Vibratory instability of cellular flames propagating in tubes. *J. Fluid Mech.* **239**, 293–307.

Rauschenbakh, B. 1961 *Vibrational Combustion*. Moscow: Mir.

Rayleigh, J. 1878 The explanation of certain acoustical phenomena. *Nature* **18**, 319–321.

Searby, G. 1992 Acoustic instability in premixed flames. *Combust. Sci. Technol.* **81**, 221–231.

Searby, G. & Clavin, P. 1986 Weakly turbulent wrinkled flames in premixed gases. *Combust. Sci. Technol.* **46**, 167–193.

Searby, G. & Quinard, J. 1990 Direct and indirect measurements of Markstein numbers of premixed flames. *Combust. Flame* **82**, 298–311.

Searby, G. & Rochwerger, D. 1991 A parametric acoustic instability in premixed flames. *J. Fluid Mech.* **231**, 529–543.

Sivashinsky, G. 1977 Nonlinear analysis of hydrodynamic instability in laminar flames. *Acta Astronaut.* **4**, 1177–1206.

Strahle, W. 1985 A more modern theory of combustion noise. In *Recent Advances in the Aerospace Sciences* (ed. C. Casci & C. Bruno), pp. 103–114. Plenum.

Williams, F. 1985 *Combustion theory*, 2nd edn. Benjamin/Cummings.

Yamaoka, I. & Tsuji, H. 1984 Determination of burning velocity using counterflow flames. In *Twentieth Symp. (Intl) on Combustion*, pp. 1883–1892. The Combustion Institute, Pittsburgh.

Zeldovich, Y. & Frank-Kamenetskii, D. 1938 A theory of thermal flame propagation. *Acta Physicochimica URSS* **IX**, 341–350.